

FIBER LOOP RING DOWN SPECTROSCOPY  
FOR TRACE CHEMICAL DETECTION

A THESIS SUBMITTED TO  
THE GRADUATE SCHOOL OF NATURAL AND APPLIED SCIENCES  
OF  
MIDDLE EAST TECHNICAL UNIVERSITY

BY

BETÜL CENGİZ

IN CONFORMITY WITH THE REQUIREMENTS  
FOR  
THE DEGREE OF  
MASTER OF SCIENCE  
IN CHEMISTRY

JANUARY, 2013



Approval of the thesis:

**FIBER LOOP RING DOWN SPECTROSCOPY FOR TRACE CHEMICAL DETECTION**

submitted by **BETÜL CENGİZ** in partial fulfillment and the requirements for the degree of **Master of Science in Chemistry Department, Middle East Technical University** by,

Prof. Dr. Canan Özgen  
Dean, Graduate School of **Natural and Applied Sciences**

\_\_\_\_\_

Prof. Dr. İlker Özkan  
Head of Department, **Chemistry**

\_\_\_\_\_

Assoc. Prof. Dr. Mehmet Fatih Danişman  
Supervisor, **Chemistry Dept., METU**

\_\_\_\_\_

Assoc. Prof. Dr. Okan Esentürk  
Co-Supervisor, **Chemistry Dept., METU**

\_\_\_\_\_

**Examining Committee Members;**

Prof. Dr. Osman Yavuz Ataman  
Chemistry Dept., METU

\_\_\_\_\_

Assoc. Prof. Dr. Mehmet Fatih Danişman  
Chemistry Dept., METU

\_\_\_\_\_

Assoc. Prof. Dr. Okan Esentürk  
Chemistry Dept., METU

\_\_\_\_\_

Prof. Dr. Ali Gökmen  
Chemistry Dept., METU

\_\_\_\_\_

Dr. Halil Berberoğlu  
Physics Dept., METU

\_\_\_\_\_

Date: 28/01/2013

I hereby declare that all information in this document has been obtained and presented in accordance with academic rules and ethical conduct. I also declare that, as required by these rules and conduct, I have fully cited and referenced all material and results that are not original to this work.

Name, Last name : **BETÜL CENGİZ**

Signature :

## ABSTRACT

### FIBER LOOP RING DOWN SPECTROSCOPY FOR TRACE CHEMICAL DETECTION

Cengiz, Betül

MS.; Department of Chemistry

Supervisor: Assoc. Prof. Dr. Mehmet Fatih Danişman

Co-Supervisor: Assoc. Prof. Dr. Okan Esentürk

January 2013, 46 page

Fiber loop ring down (FLRD) spectroscopy is a sensitive spectroscopic technique that is based on absorption and it is convenient for trace chemical detection. Different FLRD systems are being improved in order to increase their sensitivity. In FLRD spectroscopy, detection of a sample is done by measuring of a leaking light at each trip within an optical cavity. Intensity of leaking light has an exponential decay where it is reduced by absorption of sample and scattering of light.

In this project, two FLRD set-ups at 1535 nm and 808 nm were designed. In both set-ups, optical fiber and optical fiber couplers are used to form a cavity. At 1535 nm, a FLRD set-up is constructed by utilizing a pulsed laser and used for characterization of thin films, various pure liquids and fluorescein solutions. Two different sensor regions are designed with free space collimators and ferrules for the measurement of thin films and liquids, respectively. The future endeavor of the set-up is improvement for reliability and reproducibility of the system. For visible and NIR regions, a fiber coupled laser with four colors as 642 nm, 785 nm, 808 nm and 852 nm laser is used to design of a FLRD set-up. 808 nm laser is selected to build a prototype of the FLRD system. The construction of a closed loop FLRD set-up is completed and the system is characterized. Ultimate aim in our project is to be able to do trace detection at visible and NIR regions where the chemical sensitivity is higher.

Keywords: Cavity ring down spectroscopy, fiber loop ring down spectroscopy, trace detection

## Öz

### ESER KİMYASAL TAYİNİ İÇİN FİBER HALKA RİNG DOWN SPEKTROSKOPİ

Cengiz, Betül

Yüksek Lisans; Kimya Bölümü

Tez Yöneticisi: Assoc. Prof. Dr. Mehmet Fatih Danışman

Ortak Tez Yöneticisi: Assoc. Prof. Dr. Okan Esentürk

Ocak 2013, 46 sayfa

Fiber halka ring down (FHRD) spektroskopisi soğurmaya dayalı hassas bir spektroskopik tekniğidir ve eser kimyasal tayini için uygundur. Farklı FHRD sistemleri geliştirilmekte ve hassasiyetlerini artırmak için çalışmalar devam etmektedir. FHRD spektroskopide bir malzemenin tayini ışığın bir optik kavitede her bir turdaki azalışının ölçümüyle yapılır. Azalan ışığın yoğunluğu malzemenin soğurması ve ışığın saçılmasıyla azaldığı yerlerde üstel zayıflamaya sahiptir.

Bu projede 1535 nm ve 808 nm 'de iki FHRD sistemi tasarlanmıştır. Her iki sistemde de, optik fiberler ve optik fiber bağlaştırmalar kavite oluşturmak için kullanılmıştır. 1535 nm'de ince filmleri, çeşitli saf sıvıları ve floresin solüsyonlarını karakterize etmek için atmalı lazer kullanılarak bir FHRD düzeneği oluşturuldu. Sırasıyla ince filmlerin ve sıvıların ölçümü için serbest alan kollimatörleri ve ferruleler ile iki farklı sensör bölgesi tasarlandı. Sistemin gelecek çalışması sistemin güvenilirliğini ve tekrarlanabilirliğini geliştirmektir. Görünür ve yakın infrared bölgeleri için bir FHRD sistemi fiber girişli 642 nm, 785 nm, 808 nm ve 852 nm olarak dört renkte lazer kullanılarak tasarlandı. 808 nm lazer FHRD sisteminin prototipini oluşturmak için seçilmiştir. Kapalı halka FHRD sistemi tamamlandı ve sistem karakterize edildi. Projenin temel amacı kimyasal hassasiyetin yüksek olduğu görünür ve yakın infrared bölgede eser tayin yapılabilmesidir.

Anahtar Kelimeler: Kavite ring down spektroskopisi, fiber halka ring down spektroskopisi, eser tayini

*To My Family*

## ACKNOWLEDGEMENTS

I would like to thank my supervisor Assoc. Prof. Mehmet Fatih Daniřman for his guidance and support throughout my master study.

I would like to express my gratitude to my co-supervisor Assoc. Prof. Okan Esentürk for being incredibly patient with me over two years, teaching about the all milestones in my project, finally and most importantly for giving precious advices in order to shape my life.

I must give respectful gratitude to Assoc. Prof. Hakan Altan and Dr. Halil Berberođlu from Physics Department at METU for their guidance and help throughout my project.

I would like to appreciate my colleagues Enis Arık, Merve Dođangün and Emine Kaya for their kind friendships and supports.

Special thanks to my dear friends Filiz Sevimli, Serap Çelikli, Baki Emre Çetindađ, Ufuk Büyükřahin, Nusret Bayhan, Hilal Yönet, Aycan Çađlar, Ali Baykara and Pınar Gökmen for their priceless friendships. They were always there and made me smile even on the worst of days.

I would also like to say a special thank you to Merve řendur for her valuable friendship. She was with me whenever I wish during my undergraduate and graduate years and I believe that she will be with me throughout happiest moments of my life.

Finally, I would like to great appreciate my parents and my brother Ersin Cengiz for their love and never ending motivations. And I would like to say a very special thank you to my sister Mediha Cengiz Çakırgöz for being my role model and my best friend. To be her little sister cannot be described with any love-word.

## TABLE OF CONTENTS

|  |      |
|--|------|
| ABSTRACT.....  | v    |
| ÖZ .....   | vi   |
| ACKNOWLEDGEMENTS .....   | viii |
| TABLE OF CONTENTS .....  | ix   |
| LIST OF TABLES .....   | x    |
| LIST OF FIGURES .....  | xi   |
| LIST OF ABBREVIATIONS.....   | xii  |
| CHAPTERS   |      |
| 1. INTRODUCTION.....   | 1    |
| 1.1. BEER LAMBERT LAW AND ABSORPTION SPECTROSCOPY .....  | 1    |
| 1.2. CAVITY RING DOWN SPECTROSCOPY.....  | 2    |
| 1.3. FIBER CAVITY RING DOWN SPECTROSCOPY.....  | 5    |
| 1.3.1. FIBER LOOP RING DOWN SPECTROSCOPY .....   | 6    |
| 2. THEORY .....  | 9    |
| 2.1. LIGHT TRANSMISSION PRINCIPLE OF OPTICAL FIBERS.....   | 9    |
| 2.2. SET-UP DESIGN OF FIBER LOOP RING DOWN SPECTROMETER .....  | 11   |
| 2.3. PRINCIPLE OF FIBER LOOP RING DOWN SPECTROSCOPY .....  | 12   |
| 3. EXPERIMENTAL .....  | 13   |
| 3.1. EQUIPMENTS USED .....   | 13   |
| 3.2. FLRD SET-UP at 1535 nm.....   | 14   |
| 3.2.1. Sensor Head Design with Free Space Collimators .....  | 16   |
| 3.2.2. Sensor Head Design with Ferrules.....   | 17   |
| 3.3. FLRD SET-UP at 808 nm.....  | 18   |
| 4. RESULTS AND DISCUSSIONS.....  | 21   |
| 4.1. FLRD SET-UPS at 1535 nm .....   | 21   |
| 4.1.1. Theoretical Results for the Closed FLRD Set-Up.....   | 21   |
| 4.1.2. Experimental Results for the Closed FLRD Set-Up.....  | 22   |
| 4.1.3. Experimental Results for the FLRD Set-up with Sensor Region Using Free Space<br>Collimators ..... | 24   |
| 4.1.4. Experimental Results for the FLRD Set-Up with Sensor Region Using Ferrules ...                    | 26   |
| 4.2. FLRD SET-UP at 808 nm.....  | 29   |
| 4.2.1. Theoretical Loss Calculations for the Closed FLRD Set-up .....                                    | 29   |
| 4.2.2. Experimental Results for the Closed FLRD Set-up .....   | 29   |
| 5. CONCLUSIONS.....  | 33   |
| REFERENCES .....   | 35   |
| APPENDICES   |      |
| A. Ring Down Signal Graphs .....   | 37   |

## LIST OF TABLES

### TABLES

|  |    |
|--|----|
| Table 1. Equipments used in the experiments .....  | 13 |
| Table 2. Splitted light percentage through the first coupler in the loop .....   | 15 |
| Table 3. Optical loss calculations to modelize a coupler .....   | 19 |
| Table 4. Averaged pulse shots and resulted ring down times for closed FLRD set up .....                                | 23 |
| Table 5. Thicknesses of amorphous silicone thin films and resulted ring down times .....                               | 26 |
| Table 6. Ring down time results for different solvents introduced between two ferrules .....                           | 27 |
| Table 7. Obtained ring down times for decalin (C <sub>10</sub> H <sub>18</sub> ) introduced to the sample region ..... | 27 |
| Table 8. First measurement results for fluorescein solutions (Set 1) .....   | 28 |
| Table 9. Second measurement results for fluorescein solutions (Set 2) .....  | 28 |
| Table 10. Third measurement results for fluorescein solutions (Set 3) .....  | 28 |

## LIST OF FIGURES

### FIGURES

|            |   |    |
|------------|---|----|
| Figure 1.  | Scheme of Beer Lambert Law of transmittance of a beam light that travels through an l width cuvette.....  | 2  |
| Figure 2.  | A general scheme of a CRDS set-up.....  | 2  |
| Figure 3.  | An exponential decay obtained from a CRD set-up .....   | 3  |
| Figure 4.  | Output exponential light decay (blue) from a CRDS set-up when (a) a pulsed laser (red) is used with a narrower width than round trip time (b) a continuous wave laser (red) is square modulated (c) a continuous wave laser (red) is modulated sinusoidally ..... | 4  |
| Figure 5.  | A linear fiber cavity ring down spectroscopy using two highly reflective elements .....   | 5  |
| Figure 6.  | A fiber loop cavity ring down spectroscopy using a section of fiber .....   | 5  |
| Figure 7.  | Total internal reflection guidance to the light in an optical fiber.....  | 9  |
| Figure 8.  | Illustration of numerical aperture .....  | 10 |
| Figure 9.  | Optical fiber modes (a) single mode step index (b) multi mode step index (c) multi mode graded index.....   | 10 |
| Figure 10. | A general scheme of a 2x2 optical fiber coupler .....   | 11 |
| Figure 11. | Schematic diagram of the FLRD set-up at 1535 nm .....   | 14 |
| Figure 12. | Illustration of coupling of laser light to the collimator lens .....  | 14 |
| Figure 13. | FLRD set-up output come to the detector is monitored on oscilloscope .....  | 15 |
| Figure 14. | Sensor head design by using free space collimators .....  | 16 |
| Figure 15. | Ring down signals obtained from FLRD at 1535 nm with a sensor head formed from two free space collimators .....   | 16 |
| Figure 16. | Sensor head design with two pigtailed ferrules .....  | 17 |
| Figure 17. | Ring down signal obtained from the FLRD system at 1535 nm with a sensor head formed with ferrules .....   | 18 |
| Figure 18. | FLRD experimental set-up at visible region .....  | 19 |
| Figure 19. | (a) Ring down signal and (b) fitted exponential decay obtained from the closed FLRD set up at 1535 nm.....  | 22 |
| Figure 20. | (a) Ring down signal and (b) fitted exponential light decay obtained from the closed FLRD set up at 1535 nm after the addition of isolator .....  | 23 |
| Figure 21. | (a) Ring down signal and (b) fitted exponential light decay obtained from the FLRD set up at 1535 nm after addition of a sensor region using free space collimators .....   | 24 |
| Figure 22. | Fitted exponential light decays of FLRD set-up with sensor region after introduced sample a) 2.14 mm glass b) 90 nm silicone on 2.93 mm glass surface c) 210 nm silicone on 2.17 mm glass surface d) 390-410 nm silicone on 2.17 mm glass surface                 | 25 |
| Figure 23. | (a) Ring down signal and (b) fitted exponential light decay obtained from the FLRD set up at 1535 nm after addition of a sensor region using ferrules .....   | 26 |
| Figure 24. | Recorded ring down trains riding on the laser pulse of the closed FLRD set up at 808 nm.....  | 30 |
| Figure 25. | Output signal of the reference laser light and light from the cavity .....  | 30 |
| Figure 26. | Output signal from the FLRD set-up after 70 kHz modulation of the laser (line in black demonstrates signal from the laser as a reference and line in red demonstrates the signal from the cavity) .....   | 31 |

## LIST OF ABBREVIATIONS

CRDS – Cavity Ring Down Spectroscopy  
CW – Continuous Wave  
DDCI – 1,1'-diethyl-4,4'-dicarbocyanine Iodide  
DMSO – Dimethyl Sulfoxide  
DPSS laser – Diode Pumped Solid State laser  
EDFA – Erbium Doped Fiber Amplifier  
FBG – Fiber Bragg Grating  
FCRD – Fiber Cavity Ring Down  
FCRDS – Fiber Cavity Ring Down Spectroscopy  
FLRD – Fiber Loop Ring Down  
GRIN Lenses – Graded Index Lenses  
HCN – Hydrogen Cyanide  
He-Ne Laser – Helium Neon Laser  
InGaAs – Indium Gallium Arsenide  
MMF – Multi Mode Fiber  
NA – Numerical Aperture  
Nd-YAG Laser – Neodymium-doped Yttrium Aluminum Garnet Laser  
PDMS – Polydimethylsiloxane  
PMMA – Polymethylmethacrylate  
Rh6G – Rhodamine 6G  
SMF – Single Mode Fiber

## CHAPTER 1

### INTRODUCTION

A fiber optic sensor is a fiber based design for physical and chemical sensing. Development of fiber optic sensors began in 1980s and continues progressively today.<sup>1</sup> The development milestones are considered to be the invention of the laser in 1950s, low loss fiber in 1970s and optical fiber amplifiers in 1980s.<sup>2</sup> Fiber optic sensors have been improved with the novel changes in light sources, optical elements, and spectroscopic techniques. In recent years a new spectroscopic technique fiber loop ring down (FLRD) spectroscopy has evolved for physical and chemical detections. Development of FLRD relies both on cavity ring down (CRD) and fiber cavity ring down (FCRD) spectroscopy techniques. The theory of all these techniques rely on measurement of the decay of light intensity within the cavity.<sup>3</sup> In CRDS applications, cavity is formed with two highly reflective ( $R > 99.9\%$ ) mirrors. The higher the reflectivity of mirrors the higher the sensitivity. Optical loss characterization of the cavity is obtained from exponential decay rate of the light intensity. Therefore, sensing is independent from intensity and its fluctuations. The decay becomes faster with an increase in absorption by a sample and scattering of light.<sup>4,5</sup>

In FCRD a cavity is formed with using two fiber mirrors or a fiber loop. Fiber Bragg gratings (FBGs) are optical fiber mirrors and constructed in a fiber to reflect particular wavelengths of light. In FLRD a section of fiber and couplers are used as a waveguide to the light and forms the cavity. Fiber dimensions in micrometers provide lower detection volumes for sensing. On the other hand, FLRD technique suffers from the intrinsic optical losses of the set-up elements.<sup>1</sup> In this thesis, low detection limits for chemical sensing is aimed with low optical losses.

This chapter will give a general assessment of the ring down spectroscopy by discussing the theoretical aspects of the techniques and by reviewing the literature. The chapter two will present the theory of the FLRD technique. The chapter three will present the experimental set-ups at 1535 nanometer and at visible region. Ultimate aim is to gain enough experience to be able to do trace detection at visible region where the chemical sensitivity is higher. The chapter four will present the experimental results and discussion. Finally, the chapter five will review the chapters as a conclusion.

#### 1.1. BEER LAMBERT LAW AND ABSORPTION SPECTROSCOPY

Every molecular species has its particular absorption of electromagnetic radiation. During this process transfer of energy to the molecule occurs, and the intensity of the incident beam decreases. Attenuation of the beam is in phase with the Beer Lambert Law. According to Beer Lambert Law, the amount of attenuation quantitatively relies on extinction coefficient ( $\epsilon$ ), the path length ( $l$ ) and concentration ( $C$ ) or the number density of the molecules.<sup>6</sup> The relation is;

$$A = \epsilon \times l \times C \quad \text{Equation (1.1)}$$

And transmittance ( $T$ ) is the ratio of the light intensity ( $I$ ) passed through a sample to the initial light intensity ( $I_0$ ) as in Figure 1;

$$T = \frac{I}{I_0} = 10^{-\epsilon l C} \quad \text{Equation (1.2)}$$

Relationship between absorption and transmittance is;

$$A = -\log_{10}\left(\frac{I}{I_0}\right) = -\log_{10}(T) \quad \text{Equation (1.3)}$$

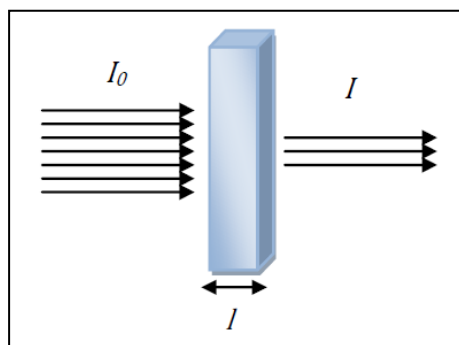


**Figure 1.** Scheme of Beer Lambert Law of transmittance of a beam light that travels through an l width cuvette

## 1.2. CAVITY RING DOWN SPECTROSCOPY

Cavity ring down spectroscopy (CRDS) is a highly sensitive absorption technique with a simple design. To construct a CRDS, a laser light is used as source and a sensitive photodetector is used as detector. A general scheme of a CRDS set-up is demonstrated in Figure 2. In a CRDS set-up light comes from the laser is coupled into the cavity that consist of two reflective mirrors. A small amount of light escaped from the second mirror is detected by a highly sensitive detector. The light exits from the cavity follows the Beer Lambert Law. Light travels between the mirrors for thousands of times and for each round, light is reduced in intensity due to the cavity losses.<sup>3</sup> Therefore, an exponential light decay is observed by the detector (Figure 3).

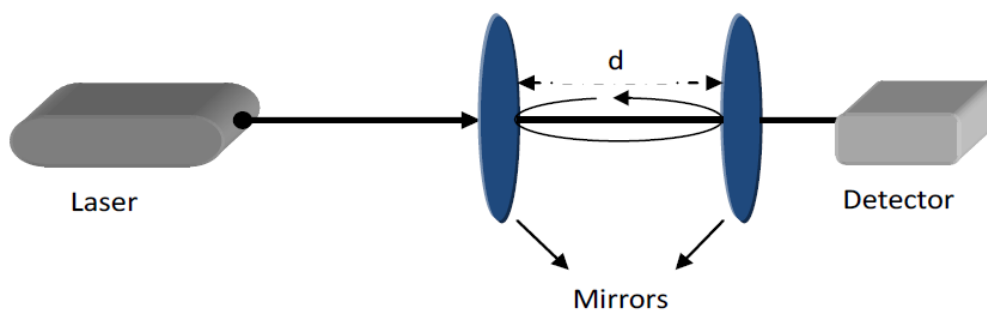


**Figure 2.** A general scheme of a CRDS set-up

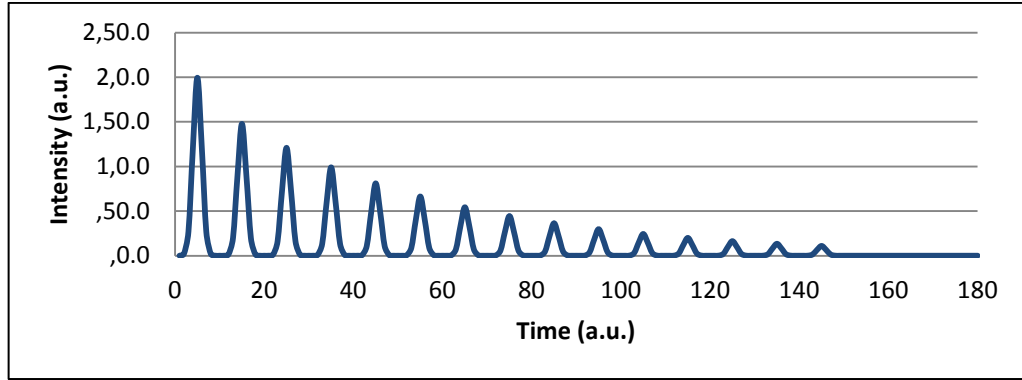


**Figure 3.** An exponential decay obtained from a CRD set-up

The time constant of the light decay can be defined as photon lifetime or ring down time of the cavity. Ring down time is the time required for the decay of an incident light to  $1/e$  of its initial intensity. It depends on all the absorption and light scattering in the cavity by mirrors and introduced sample.<sup>7</sup> Ring down time,  $\tau$ , can be defined as;

$$\tau = \frac{t_r}{A} \quad \text{Equation (1.4)}$$

where  $t_r$  is round trip time of the cavity and depends on cavity length ( $L$ ), refractive index of the medium ( $n$ ), and speed of light ( $c$ ). Thus,  $\tau$  becomes;

$$\tau = \frac{nL}{cA} \quad \text{Equation (1.5)}$$

Output exponential signal of any CRDS set-up depends on the relation between the pulse width of the laser light and the round trip time of the system. If a pulsed laser is used and width of the injected pulse is shorter than the round trip time, exponential light decay is obtained as pulses (Figure 4a). When a continuous wave (CW) light source is square modulated, exponential light decay follows the end of the laser pulses. Similarly, an exponential light decay is observed if a continuous light is switched quickly (Figure 4b). Time resolved CRDS is not preferred when the repetition rate of the laser is higher than the 10 kHz and output ring down time is longer than 10  $\mu$ s.<sup>8</sup> Therefore, phase shift in frequency domain is an alternative technique for CRDS applications. In phase shift technique a CW light is modulated sinusoidally and a phase delay is obtained between the light enters the cavity and exits from the cavity (Figure 4c). The delay of the phase arises from the losses in the cavity and it is related to ring down time. Phase shift ( $\phi$ ) is related with decay time ( $\tau$ ) of the excited state;

$$\tan(\phi) = -\omega\tau \quad \text{Equation (1.6)}$$

where  $\omega$  is the modulation frequency. Equation (1.6) is improved by the addition of an offset angle ( $\phi_0$ ). The offset angle is derived from the loss of the empty cavity, and the loss of the set-up elements. Characterization of the set-up is done by the determination of the offset angle. When the offset angle is subtracted from the total phase shift, delay derived from the ring down time is found.<sup>9</sup> Thus Equation (1.6) becomes;

$$\phi = \phi_0 - \arctan(\omega\tau) \quad \text{Equation (1.7)}$$

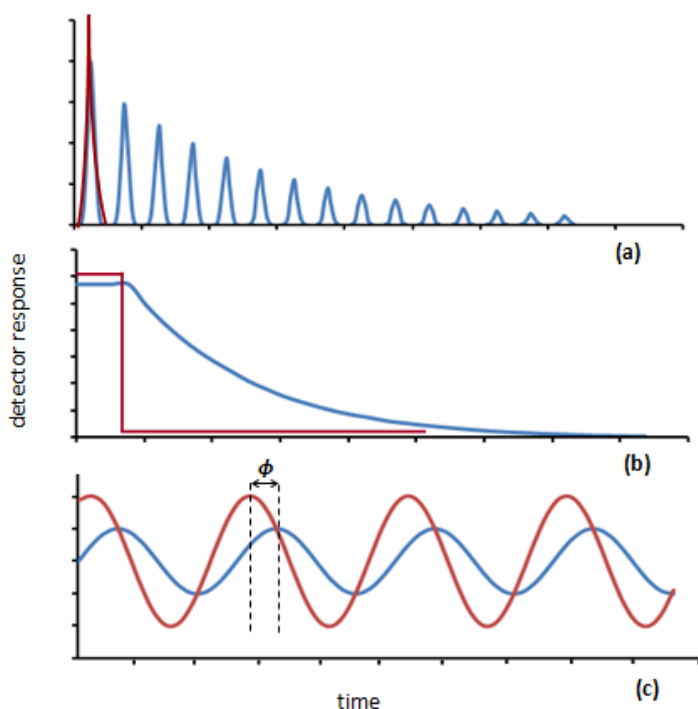


**Figure 4. Output exponential light decay (blue) from a CRDS set-up when (a) a pulsed laser (red) is used with a narrower width than round trip time (b) a continuous wave laser (red) is square modulated (c) a continuous wave laser (red) is modulated sinusoidally**

Different implementations of CRDS have been studied for three decades. The origin of CRDS technique started with characterization of high reflectivity mirrors for aerospace industry.<sup>10-12</sup> The first reported spectroscopic application was done by Deacon and O'Keefe.<sup>4</sup> In this study, a closed optical cavity consist of highly reflective mirrors was used for measurements of absorption of a gaseous molecular oxygen with using a pulsed laser.

Lehman and Romanini investigated the several overtones of HCN gas by CRDS.<sup>13,14</sup> They achieved an amazing instrument resolution of  $7 \times 10^{-10} \text{cm}^{-1}$  for the absolute absorption coefficient of the species. Later a hollow cathode source as a part of a pulsed CRDS system was used by Kotterer *et al.* for the determination of molecular ions absorption.<sup>15</sup> On the other hand, first continuous wave CRDS set-up was designed by Anderson *et al.*<sup>12</sup> In their study, they used He-Ne laser to measure the reflectivity of low loss high reflective mirrors. A similar cw-CRDS set-up was constructed by Romanini *et al.* in 1997.<sup>16</sup> They used a dye laser and acousto-optic modulator for pulsing to measure the overtone transition of  $\text{C}_2\text{H}_2$  (acetylene) around 570 nm at low pressure. They achieved a great sensitivity of  $10^{-9} \text{cm}^{-1}$  as noise (rms) equivalent absorption.

In 1933, according to the study of Duschinsky phase shift is obtained from the difference frequency of intensity modulated light and frequency of light after fluorescence.<sup>17</sup> In the study of Engeln *et al.* ps-CRDS was used for measurement of transition frequencies of  $^{18}\text{O}_2$ .<sup>18</sup> According to their study, the highest sensitivity is obtained when  $\phi$  is at 45 degrees ( $\tan\phi = 1$ ). This technique was applied to fiber loop ring down spectroscopy by Loock *et al.* in 2004.<sup>9</sup> Their study demonstrated that phase shift FLRD spectroscopy can be applicable as an absorption set-up designed for any flow system. They measured the phase angle as a function of concentration of 1,1'-diethyl-4,4'-dicarbocyanine iodide in dimethyl sulfoxide and the determined detection limit as around 6  $\mu\text{M}$  for a 30-40  $\mu\text{m}$  absorption path.

### 1.3. FIBER CAVITY RING DOWN SPECTROSCOPY

Fiber cavity ring down spectroscopy (FCRDS) is an implementation of CRDS. In a FCRDS set-up fiber mirrors or a section of optical fiber is used as a waveguide (cavity) instead of high reflectivity mirrors used in CRDS.<sup>3,8</sup> An optical fiber is used for the transmission of light and leaking of light through the fiber is used to measure the properties of the FLRD systems. Here, I will introduce and then discuss the FCRDS.

Fiber cavity ring down spectroscopy can be classified into two groups according to cavity features; linear and loop fiber cavities. Linear fiber cavities consist of fiber mirrors (Figure 5) and fiber loop cavities consist of a section of fiber (Figure 6).<sup>8</sup>

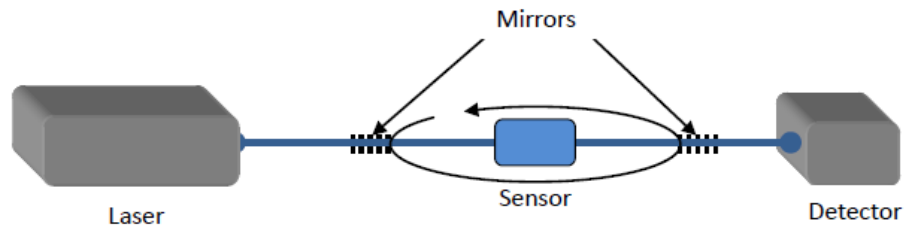


**Figure 5.** A linear fiber cavity ring down spectroscopy using two highly reflective elements

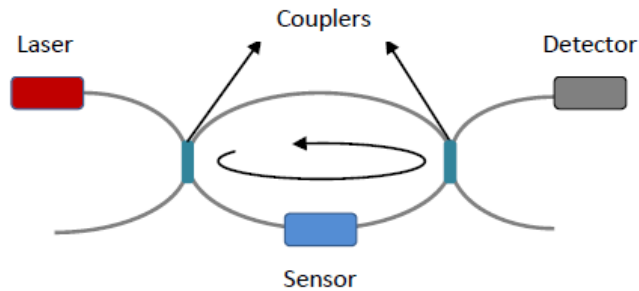


**Figure 6.** A fiber loop cavity ring down spectroscopy using a section of fiber

To construct a linear FCRDS set-up, fiber Bragg gratings (FBGs) are used. A fiber Bragg grating is a reflector used in optical fibers. It consists of multiple layers with various refractive indexes. Fiber Bragg gratings can be used to filter certain wavelengths or to reflect specific wavelengths.

In the study of Gupta *et al.* FBGs were the reflective elements of the FCRDS set-up at 1563.6 nanometer.<sup>19</sup> Their set-up cavity involved a 10 meter long single mode fiber (SMF) that contained FBGs at the ends of the fiber. They achieved 2.3 % optical loss for each round trip of the laser light through the set-up. Trefiak *et al.* presented a study for micro fluid measurements with using both fiber linear and fiber loop FCRDS set-ups.<sup>20</sup> For the fiber linear cavity set-up they used FBGs at the ends of a 70 meters long SMF. For the fiber loop set-up they used an 80 meters long multi mode fiber (MMF) with 99:1 couplers to guide light into the loop. Then, absorption spectrum of cyanine dye was measured with phase shift technique. They achieved lower optical losses for the linear FCRDS set-up, however FBGs leads to the light reflection in a certain range of wavelengths.

### 1.3.1. FIBER LOOP RING DOWN SPECTROSCOPY

Fiber loop ring down (FLRD) spectroscopy is a highly sensitive absorption technique.<sup>3</sup> Design of a general FLRD set-up includes a laser light source, fiber and a sensitive photo detector. Light is coupled into the system with optical fiber couplers with high split ratios such as 99:1. Light transmission principle through the set-up is similar to the CRDS technique. Light travels through the loop for hundreds of times and for each round a small fraction of it exits the loop and is detected with reduced intensity as an exponential light decay. Cavities of FLRD designs provide broadband working range of wavelengths. Therefore light transmission through the loop relies on fiber optic material and each components of the cavity. In general, FLRD systems can be formed with multiple sensor regions in one set-up and easily configured to sense various chemical and physical properties with inexpensive and simple designs.

The first reported FLRD study was presented by Stewart *et al.* in 2001 for chemical sensing at near IR region.<sup>21</sup> They used a 5 cm length of gas cell for the sensing of methane and 50 meter loop that includes an erbium doped fiber amplifier (EDFA) to prevent high optical loss of the cell. However, the stability of the amplifier was not good enough. Therefore, detection of the ring down time became complicated. In the literature, studies on FLRD demonstrated that non amplified systems are more stable compare to the amplified ones.<sup>22</sup> In 2002, a non amplified system was designed by Brown *et al.* with a pulsed Nd:YAG pumped dye laser. They constructed a sample cell as 3.8  $\mu\text{m}$  length and introduced their sample. They achieved a detection limit for 1,1'-diethyl -4,4'-dicarbocyanine iodide (DDCI) in dimethylsulfoxide (DMSO) in absorptivity ( $\epsilon\text{C}$ ) as  $100\text{ cm}^{-1}$ . In 2003, they presented their improved results by the enhanced configuration of the sensor region.<sup>23</sup> In this study, they placed a hair in polydimethylsiloxane (PDMS) polymer and cured it for 24 hours. Then, the hair was removed and a 47  $\mu\text{m}$  microchannel was obtained. They achieved a detection limit as  $10^{-10}$  mol, or  $7 \times 10^{-8}$  g DDCI in DMSO.

In 2004, Tarsa *et al.* designed a FLRD set-up at near infrared region.<sup>24</sup> Their set-up design included a 2.2 km SMF and two 99:1 couplers as resonator. To obtain an evanescent wave sensor region, they formed a tapered region that is 10  $\mu\text{m}$  in waist diameter and 28.0 mm in length. Ring down time measurements were done both by using a pulsed laser at 1550 nm and by a CW laser at 1520 nm. They achieved ring down times for pulsed and CW set-ups as  $48.98 \pm 2.50\ \mu\text{s}$  and  $52.28 \pm 0.38\ \mu\text{s}$  respectively. They measured the 1-octyne and detected a minimum concentration as 0.049% per  $\sqrt{\text{Hz}}$ .

FLRD technique was used as a pressure sensor by Wang and Scherrer in 2004.<sup>25</sup> Their set-up consist of CW diode laser at 1650 nm, a 61 meter long SMF, two 2x1 couplers with a 99:1 split ratio, and a photo detector. To form a sensor region a piece of fiber independent from the set-up was placed parallel to fiber in the loop and a lightweight aluminum plate was placed onto the fibers as a upside-down "u" shaped platform ( $\Pi$ ). They applied pressure between 0 to  $9.8 \times 10^6$  Pa and recorded the results during loading and unloading pressure to the platform. In 2005, Wang designed a fiber Bragg grating loop ring down (FBG-LRD) set-up to sense temperature.<sup>26</sup> When FBGs involved in FLRD set-up, the FBGs resulted in additional optical losses and, therefore, temperature sensing of FBGs can be obtained from the ring down time measurements. Ring down time decreased to 3.1  $\mu\text{s}$  from 4.4  $\mu\text{s}$  when the fiber sensor part between the FBGs was heated. His study demonstrated that FLRD set-up can be used as temperature sensor up to 593  $^{\circ}\text{C}$  with high sensitivity and low cost.

In 2006, Li *et al.* constructed a FLRD set-up with a sensor head as capillary-fiber interface.<sup>27</sup> To design the sensor region, they mechanically drilled a capillary with a size of 150  $\mu\text{m}$  and embedded it in polymethylmethacrylate (PMMA) polymer plate. Then they drilled another 150  $\mu\text{m}$  hole perpendicular to the capillary and two ends of the fiber were placed into these holes. Absorption path was adjusted as 30  $\mu\text{m}$ , fiber ends were aligned, and then these parts were fixed with epoxy. The aim of this study was detection of capillary electrophoresis of biomolecules at

near infrared region. In 2009, a similar set-up at 405 nm with using a low loss UV fiber was designed by Waechter *et al.*<sup>28</sup> Their design involved a sensor head made from a PMMA plate with two grooves. One groove was used for introducing two fiber ends within 190  $\mu\text{m}$  distance and the other one was used for delivery of fiber placed at  $6^\circ$  angle from the gap. Glass capillaries were placed to the entrance and exit holes for the sample transportation. They measured myoglobin, tartrazine and proposed pharmaceutical ingredient containing pyrole, benzodiazepine, imidzole, and piperidinylcarbonyl. The detection volume of the set-up was 6 nL and the minimum detectable concentrations of myoglobin, tartrazine and pharmaceutical ingredients was 1  $\mu\text{M}$ , 5  $\mu\text{M}$  and 20  $\mu\text{M}$  respectively.

Recently, Rushworth *et al.* has designed a FLRD set-up for the analysis of small volume liquid samples.<sup>29</sup> They configured a novel coupler based on a  $45^\circ$  reflective notch polished between the fibers and provides nearly 100% coupling. A capillary tube was placed underneath of the end of the cleaved fiber ends. To introduce sample to the gap a meniscus was formed at the top of the tube. Aqueous rhodamine 6G (Rh6G) was measured at 532 nm. Detection limit was found as  $0.11 \text{ cm}^{-1}$ . For Rh6G it corresponded to 0.93  $\mu\text{M}$  in a volume of 19 nL.

This thesis study includes two FLRD set-up designs one at 1535 nm and the other one at 808 nm. For the set-up at 1535 nm a pulsed laser, a section of single mode fiber, two 2x2 couplers with 99:1 split ratio, and a photodiode were used. At this wavelength optical loss is very low and this provides enhanced sensitivity. Different sensor head configurations and their results will be given in the Chapter 3. At 808 nm, a fiber coupled diode laser, a section of single mode fiber, two 2x2 couplers with 98:2 split ratio and a photodiode were used. Design of the set-up will be detailed in the Chapter 3.



## CHAPTER 2

### THEORY

This chapter is presented to evaluate the fiber loop ring down (FLRD) spectroscopy from theoretical aspect. First the principle of light transmission through an optical fiber is given. Then the characteristic features of FLRD set-up elements will be mentioned. Finally general principle of FLRD technique will be described.

#### 2.1. LIGHT TRANSMISSION PRINCIPLE OF OPTICAL FIBERS

An optical fiber is made of glass or plastic and used for light transmission. Light is guided through an optical fiber according to total internal reflection phenomenon. When a light ray comes on an interface between two mediums with different refractive indexes refraction occurs. This is described by Snell's Law for refraction<sup>6</sup>;

$$n_1 \sin \theta_1 = n_2 \sin \theta_2 \quad \text{Equation (2.1)}$$

Where  $n_1$ ,  $n_2$  are refractive indexes of the mediums and  $\theta_1$ ,  $\theta_2$  are ray angles to the normal of the interface. When a ray comes on the interface with an angle larger than the critical angle and the refractive index of medium on the other side is lower, total internal reflection occurs. For an optical fiber refractive index of cladding is lower than refractive index of core and light is kept in the core.

A standard optical fiber is made of silica and has two parts as core and cladding. These parts are surrounded by a plastic coating that protects the inner parts of the fiber. Light is guided in the core and cladding. The refractive index of core is higher than cladding that allows guiding of light through the fiber. For different applications different core and cladding diameters are available. In simple terms, optical fibers can be classified according to their core and cladding diameters. For single mode fibers (SMF) core/cladding diameters are usually around 9/125  $\mu\text{m}$  and for multi mode fibers (MMF) core/cladding diameters are around 100/140  $\mu\text{m}$ .<sup>30</sup> Light travels through the fiber as electromagnetic waves and, total internal reflection at the interface between the core and cladding keeps the light inside the core (Figure 7).<sup>31</sup>

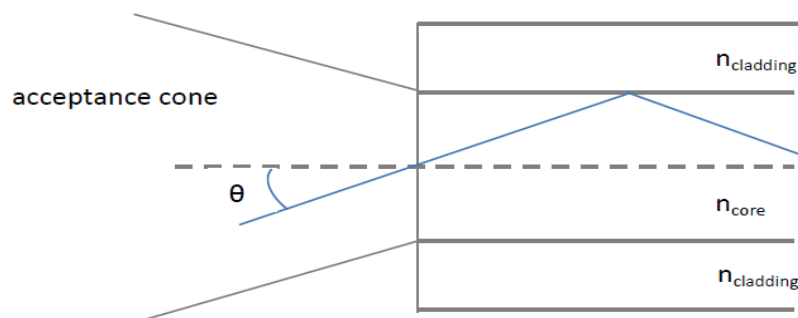


**Figure 7.** Total internal reflection guidance to the light in an optical fiber

Light from free space is coupled into the fiber according to its acceptance angle as in Figure 8. This angle can be defined as numerical aperture (NA) of the fiber;

$$\theta = \arctan\left(\frac{D}{2a}\right) \quad \text{and} \quad NA = \sin\theta \quad \text{Equation (2.2)}$$

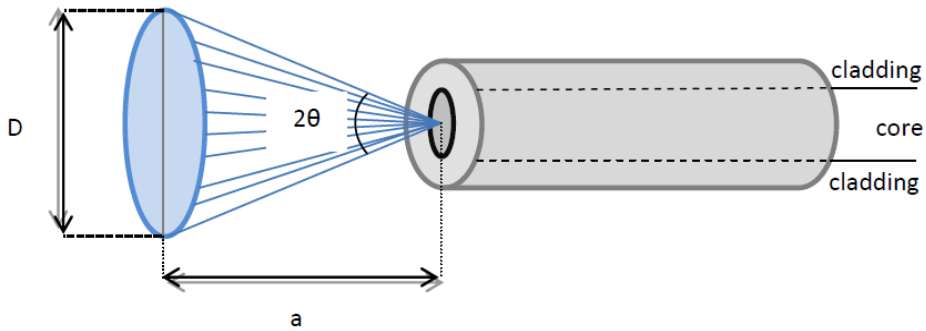


**Figure 8.** Illustration of numerical aperture

Fibers can be classified in three groups as single mode step index, multi mode step index and multi mode graded index fiber.<sup>30</sup> For single mode fibers light is guided through a path, on the other hand for multi mode fibers light can be guided through paths more than one. Throughout a step index fiber refractive index is the same, while the refractive index of graded index fiber is variable (Figure 9).

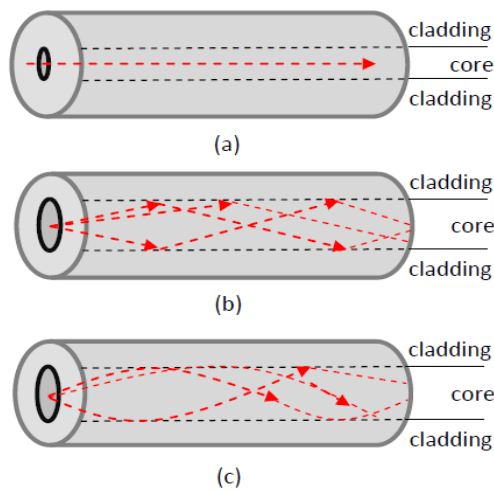


**Figure 9.** Optical fiber modes (a) single mode step index (b) multi mode step index (c) multi mode graded index

When light transmit through a fiber, it is reduced in intensity with distance. This reduction is called as attenuation and measured in decibel (dB) unit. dB is a logarithmic unit that describes a ratio of physical quantity relative to a determined reference level. When dB refers the light intensity measurement, a ratio can be defined as ten times of ten base logarithm of the ratio of the measured to reference quantity;

$$\alpha_{dB}L = 10\log_{10}\left(\frac{I}{I_0}\right) \quad \text{Equation (2.3)}$$

where  $\alpha_{dB}$  is light intensity attenuation per unit length in dB,  $L$  is fiber length,  $I_0$  is incident light intensity, and  $I$  is the reduced light intensity. Light intensity decreases through a fiber due to absorption, scattering, impurities, bending, and; therefore, each fiber has a specific attenuation coefficient.

## 2.2. SET-UP DESIGN OF FIBER LOOP RING DOWN SPECTROMETER

A fiber loop ring down (FLRD) spectroscopy set-up can be designed simply with inexpensive components.<sup>32</sup> The main components are a light source, fiber, and a detector to construct a FLRD set-up. As a light source an inexpensive laser with low power in miliwatts can be used at various wavelengths. Optical fibers are broadband and, can be used with lasers at different wavelengths. To design a loop, initially a laser light is coupled into a fiber. During this process, an optical fiber coupler is used to transmit and split the light. A fiber coupler is an optical device with one or more inputs and one or more outputs (Figure 10). Distribution of light power relies on the wavelength and polarization of the fiber. It can be fabricated with different ways as twisting, fusing, and tapering of fibers. A single mode fiber coupler with more than one input and with only one output at a certain wavelength is not preferred due to a high insertion loss in the FLRD systems, in general.



**Figure 10.** A general scheme of a 2x2 optical fiber coupler

In this study a fiber loop is constructed by fusion technique that uses a cleaver and a splicer. The first step of this process is stripping of fiber sections that will be spliced from their protective coatings using a stripper. Then, the open fiber ends are cleaned by using tissue papers and a pure solvent such as alcohol or acetone. After cleaning, ends of the fibers are cleaved with a cleaver. The cleaned and cleaved fiber ends are placed into the splicer for fusion. The part of the splicer where fusion occurs consists of two fixtures to fix the end of the fibers and two electrodes. The fusion splicing process is done by heating with an electric arc. Stripped part of the fiber can be recoated by the splicer heater mode. Fusion loss and proof test are obtained from splicer. The aim for fusion splicing of optical fibers is to minimize scattering or reflection losses during the light transfer from a fiber to another fiber piece.

Alternative methods to get fibers connected are mechanical splicing and use of connectors. However, these result in much higher optical losses compared to fusion splicing. Splicing must be

done very carefully, because any interference can result in splicing with high optical losses or bubbles on the fiber. Fiber ends should not be touched or touch to any surface. The fiber ends should be placed co-linearly into the splicer.

To detect the light signal a highly sensitive photo diode is used for complete design of FLRD. Diodes are designed for specific aims as PIN structure and can be packaged with a fiber connection.

### 2.3. PRINCIPLE OF FIBER LOOP RING DOWN SPECTROSCOPY

For a FLRD set-up, light is coupled into a fiber loop and travels within the loop for many rounds until it leaks to zero intensity.<sup>3,7,8</sup> At each round, a small fraction of light is leaked to a photo detector and the rest of the light continues to travel through the loop with an optical loss. The output signal on the detector is monitored by an oscilloscope and recorded. The recorded signal is an exponential decay of intensity of the light within the cavity. The decay of light intensity as the time passes is given;<sup>8</sup>

$$\frac{dI}{dt} = - \frac{IAc}{nL} \quad \text{Equation (2.4)}$$

In Equation (2.4),  $I$  is light intensity at time  $t$ ,  $A$  is total internal transmission loss of the light for each round,  $c$  is the speed of light,  $n$  is the refractive index of the medium, and  $L$  is the length of the fiber loop. The total loss,  $A$ , is a sum of all transmission losses such as the fiber absorption and scattering losses, coupler insertion losses, loss through the connectors, and sample absorption, if any. Integration of Equation (2.4) results an exponential intensity change with time;

$$I = I_0 e^{-\left(\frac{Act}{nL}\right)} \quad \text{Equation (2.5)}$$

where,  $I_0$  is initial light intensity that is coupled into the cavity. The Equation (2.5) indicates that  $A$  is independent from fluctuations of initial light intensity since the decay rate of light intensity is measured instead of absolute intensity.

Equation (2.5) is solved to define ring down time,  $\tau_0$ , that is the time required for the decay of an incident light to 1/e of its initial intensity.

$$\tau_0 = \frac{nL}{cA} \quad \text{Equation (2.6)}$$

For an empty FLRD set-up,  $A$  is defined as total internal transmission loss and it is inversely proportional to ring down time. If there is an external act like a physical change as pressure, temperature, stress or a sample addition to the sensor head, its loss effect,  $B$ , is added to total transmission loss and therefore ring down time changes.

$$\tau_0 = \frac{nL}{c(A + B)} \quad \text{Equation (2.7)}$$

## CHAPTER 3

### EXPERIMENTAL

In this chapter, a general assessment will be given about two FLRD system set-ups designed at 1535 nanometer and visible region. Some of the equipments such as scope, detector, power meters etc. are common and only listed in one.

#### 3.1. EQUIPMENTS USED

Equipments used for the design of the two FLRD set-ups are listed in Table 1. (Item numbers will be used in schematic diagram of the set-ups and in the text.)

**Table 1.** Equipments used in the experiments

|                |    | <b>Optical element</b> | <b>Company</b>            | <b>Model</b>             | <b>Description</b>  |
|----------------|----|------------------------|---------------------------|--------------------------|---|
| <b>1535 nm</b> | 1  | Laser                  | Cobolt                    | CoboltTango™-Lab         | Pulsed 1535 nm diode-pumped solid-state (DPSS) Laser                            |
|                | 2  | Lens                   | -                         | -                        | Coupling of laser light into the fiber  |
|                | 3  | Fiber Coupler          | Lightel                   | SWC-22-P-9901-H-1-B-0    | @1535 nm, 2x2 ports, 99:1 split ratio   |
|                | 4  | Fiber                  | Domino                    | SM.G.652.D               | 0.25 dB/km attenuation at 1535 nm   |
|                | 5  | Isolator               | Lightel                   | TIS-01-A-B-0             | hybrid 1550 nm 1% tap coupler   |
|                | 6  | Detector               | Electro-Optics Technology | ET-3010                  | InGaAs PIN Detector   |
|                | 7  | Oscilloscope           | Lecroy                    | 6100A                    | 1 GHz, 4 Channel Scope  |
|                | 8  | Power meter            | Thorlabs                  | PM100D                   | Wavelength range: 185 nm - 25 μm<br>Power range: 100 pW to 200 W                |
|                | 9  | Power sensor           | Thorlabs                  | S310C                    | Thermal sensor, surface absorber, wavelength range: 0.19 - 25 μm, 10 W          |
|                | 10 | Lens                   | Thorlabs                  | 50-1550A                 | Free space collimation  |
|                | 11 | Ferrule                | Thorlabs                  | SMPF0215                 | Pigttailed, Ø1.8 mm, 0°, Antireflective coated: 1550 nm                         |
| <b>808 nm</b>  | 12 | Laser                  | Thorlabs                  | MCLS1                    | Fiber coupled diode laser with 4-wavelength channels (642, 785, 808 and 852 nm) |
|                | 13 | Fiber Coupler          | Lightel                   | SWC-22-P-9802-0808-1-L-1 | @808 nm 2x2 ports, 98:2 split ratio   |
|                | 14 | Fiber                  | Nufern                    | 780HP                    | 3 dB/km attenuation at 808 nm   |
|                | 15 | Function Generator     | Kenwood                   | FG-273                   | 0.02 Hz to 2MHz   |
|                | 16 | Detector               | Thorlabs                  | PDB210A                  | Silicone- PIN detector  |

### 3.2. FLRD SET-UP at 1535 nm

To gain experience, a FLRD set-up was designed at 1535 nm as in Figure 11.

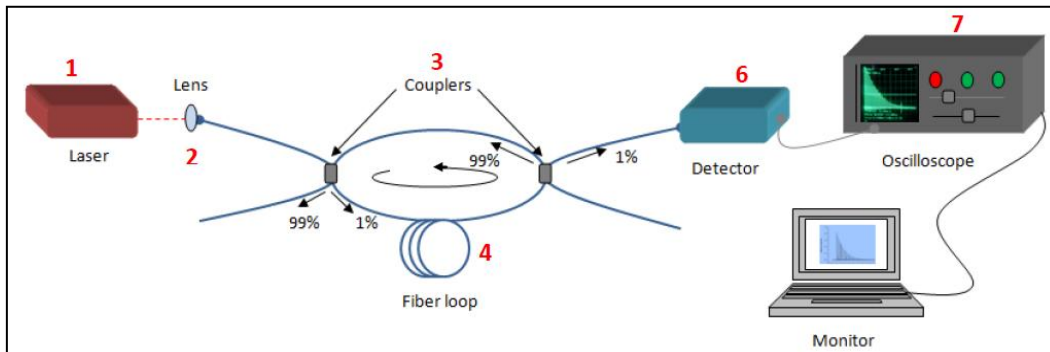


**Figure 11.** Schematic diagram of the FLRD set-up at 1535 nm

The light source of the system was a diode-pumped solid-state laser (DSSL) (1) at a fixed wavelength  $1535 \pm 2 \text{ nm}$ . It produces  $4 \pm 1 \text{ ns}$  pulses at a repetition rate of  $3 \pm 1 \text{ kHz}$ . Light was coupled into the fiber with free space coupling method using a collimator lens (2). First, the light beam received from the laser was aligned parallel to the surface of the optical table with two irises at the same height that are placed in near-field (close) and far field from the laser. When the light passed through the center of irises with same height on the table, the path of light beam became parallel to the table surface.

After the beam alignment procedure, a fiber end collimator lens on a XYZ stage was placed in front of the laser for free space coupling to achieve optimum light coupling into the fiber. During optimization the coupled light power was monitored with the power meter (8) from the fiber end of the lens. As a sensor element, thermal power sensor (9) was used to measure optical power of laser light (Figure 12).

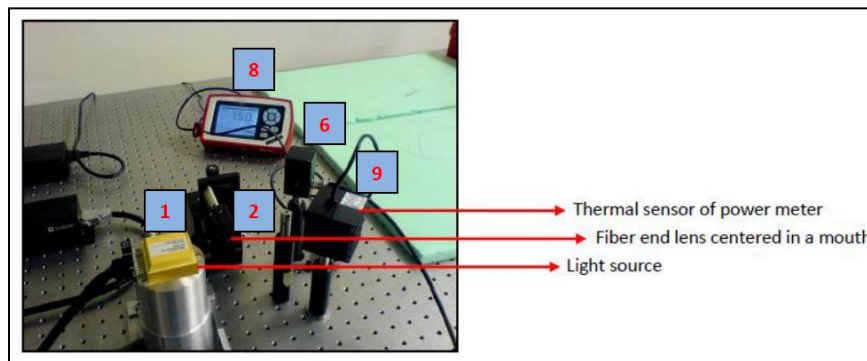


**Figure 12.** Illustration of coupling of laser light to the collimator lens

Next step was connecting a 2x2 fiber coupler (3) to the fiber end of the lens by fusion splicing. Split ratio of the coupler was selected as 99:1. The insertion losses given by the manufacturer are  $\leq 0.17 \text{ dB}$  and  $\leq 20.47 \text{ dB}$  for 99% and 1% legs, respectively. The split ratios of the couplers were selected according to length and attenuation of the fiber. Only, 1% of light that is delivered from

the lens get into the loop and for the next rounds 99% of the light in the loop continues to travel through the set-up. The reason for the selection of 1% coupling as opposed to 99% is because the attenuation results a much lower light intensity if 99% is chosen. A comparison of power of the light as percentage splitted as 99:1 by first coupler is demonstrated in Table 2 for several rounds in the loop. As seen, the intensity of light in the loop becomes equal at the end of the 1<sup>st</sup> round and 1% leg always has a much higher intensity in the loop at every other following rounds.

**Table 2.** Splitted light percentage through the first coupler in the loop

| <i>P: power of the light</i>          | 99% port (percentage) | 1% port (percentage) |
|---------------------------------------|-----------------------|----------------------|
| Initial power                         | 99P%                  | P%                   |
| Reduced power @ 1 <sup>st</sup> round | 0.99P%                | 0.99P%               |
| Reduced power @ 2 <sup>nd</sup> round | 0.0099P%              | 0.9801P%             |
| Reduced power @ 3 <sup>rd</sup> round | 0.000099P%            | 0.970299P%           |

After the connection of the coupler to the collimator the loop can be prepared by the addition of the fiber cavity as shown in Figure 11. The first set-up was done by addition of 20 meter fiber (4) by splicing the fiber to the 1% leg of the coupler. Next a second coupler was added to the set-up by splicing the other end of 20 meter fiber to the input fiber end of the coupler. Finally, the 99% leg of the second coupler was spliced to the other second input of the first coupler. With this final connection the fiber cavity is formed. The decay in the fiber cavity was monitored from the 1% leg of the second coupler. To sense the light, an InGaAs PIN detector (6) was placed to the 1% output of the second coupler and to connect the fiber and detector a fiber end connector was spliced to the coupler fiber end. Then, a 1 GHz digital oscilloscope was connected to the detector to monitor the output signal of the system (Figure 13). The prototype of the set-up was characterized. Unfortunately, several problems such as intensity fluctuations and back reflections were revealed. To solve these problems and improve the set-up second coupler was replaced with an isolator (5).

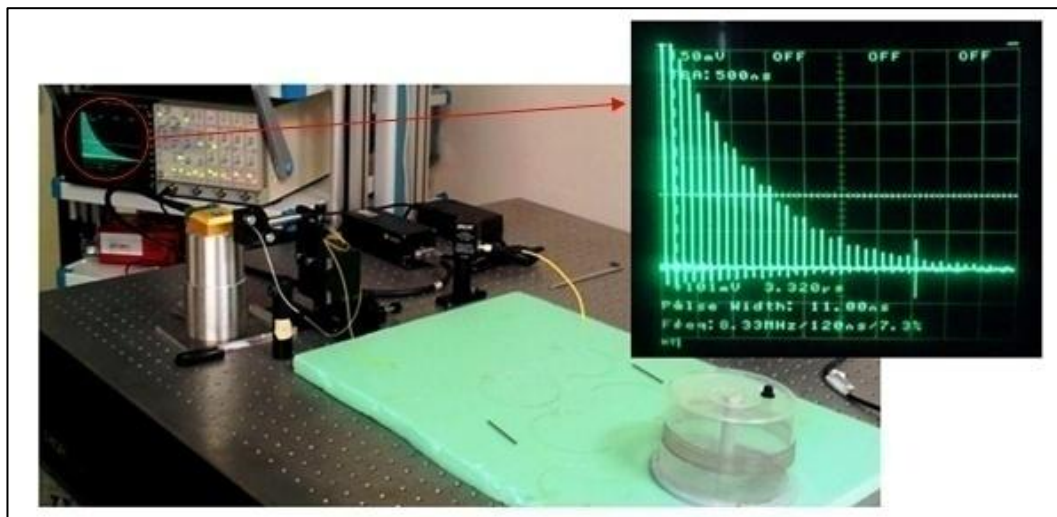


**Figure 13.** FLRD set-up output come to the detector is monitored on oscilloscope

### 3.2.1. Sensor Head Design with Free Space Collimators

In FLRD systems, different sensor heads can easily be configured for both chemical and physical sensing. In this study, first a sensor head with two free space collimators (10) was designed after the characterization of closed fiber loop set-up. Free space collimators are fiber end graded index (GRIN) lenses used for collimating light from a fiber output and coupling light into a fiber. To construct sensor head, collimators were placed between the coupler and the isolator (Figure 14). Then, coupling of light was optimized by changing the relative positions of lenses via a translational stage and with special mounts that lenses were centered in it. After optimization of coupled light that passed through the sensor region, ring down data was recorded and monitored on the oscilloscope (7) as in Figure 15. Fitting process of the output signal was done by Origin and ring down time was obtained from the fit equation.

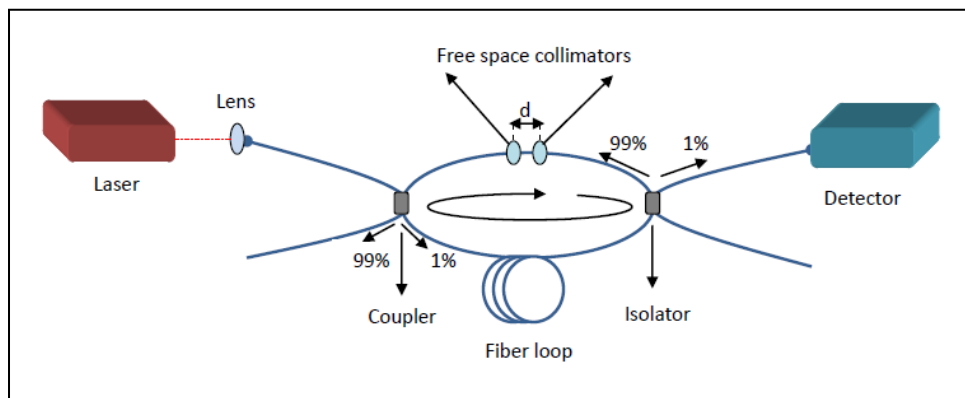


Figure 14. Sensor head design by using free space collimators

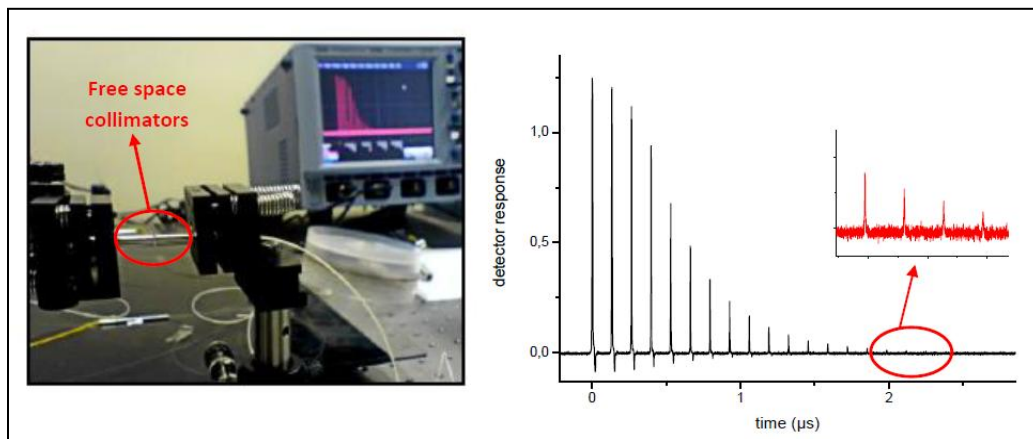


Figure 15. Ring down signals obtained from FLRD at 1535 nm with a sensor head formed from two free space collimators

Sensor head allowed introduction of a sample between the collimators. In this thesis, thin amorphous silicone films on glass with different thicknesses were placed between the collimators. The thicknesses of glasses were 2.17 mm and 2.93 mm. The thicknesses of

amorphous silicon were 210 nm and 390-410 nm on 2.17 mm glass and 90 nm on 2.93 mm glass. For each sample ring down data was recorded by the oscilloscope. The results will be discussed in the Chapter 4.

### 3.2.2. Sensor Head Design with Ferrules

Sensor head configurations are determined by the properties of samples. For liquid measurements another sensor head was designed with the use of ferrules (11). The ferrules are fiber pigtailed GRIN lenses with 1.8 mm in diameter. To configure the sensor region, ferrules were placed between the coupler and isolator as in Figure 16. First, one of the ferrules was fixed in the center of a special mount and the other one centered in another mount that is placed on a XYZ translational stage. Then, distance between the ferrules was adjusted with micrometer on Z axis of stage and light was coupled. A reference distance between the ferrules was adjusted relative to touching distance of the ferrules.

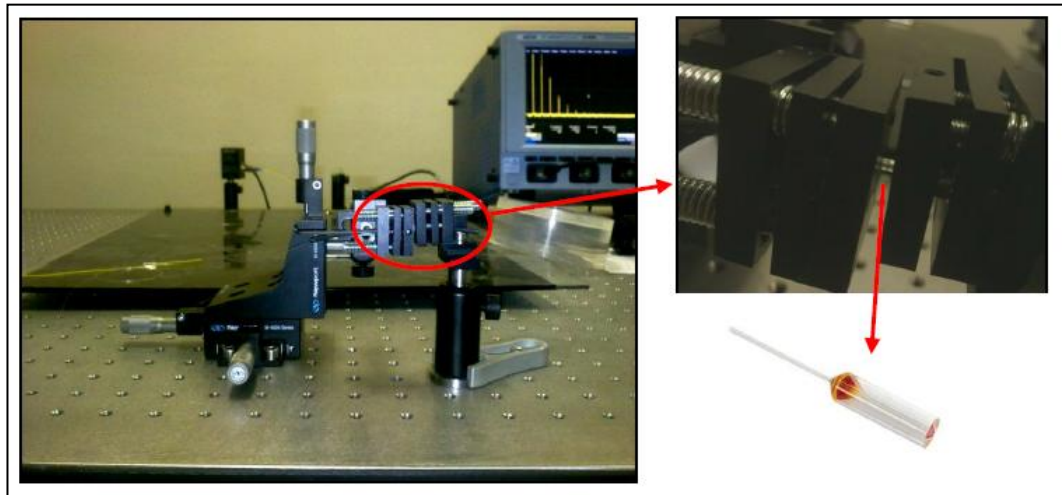


**Figure 16.** Sensor head design with two pigtailed ferrules

Optimization of the sensor head was done when distance between the ferrules was set to 80  $\mu\text{m}$ . The ring down data was obtained and monitored on the oscilloscope before introducing a sample in the region (Figure 17).

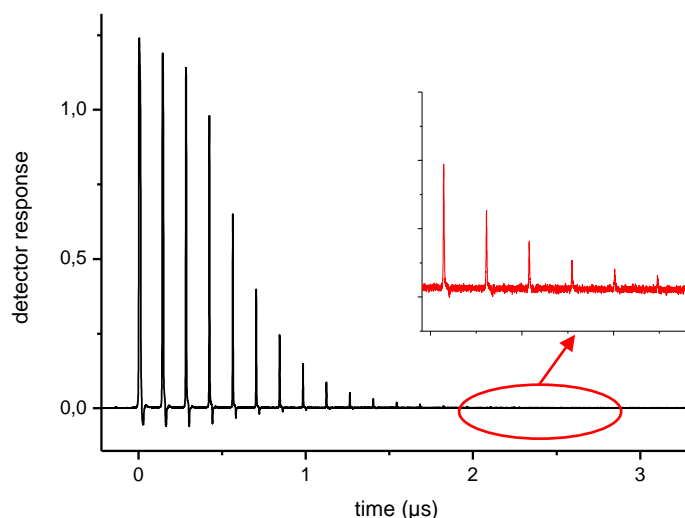


**Figure 17.** Ring down signal obtained from the FLRD system at 1535 nm with a sensor head formed with ferrules

To test the set-up for absorption measurement, sensor cavity was filled with various solvents. Ring down data was recorded for water, isopropyl alcohol, n-butanol, n-hexane and decaline that are introduced between the ferrules with a syringe. In addition, different concentrations of fluorescein in water were measured and ring down data was recorded with the same method.

### 3.3. FLRD SET-UP at 808 nm

FLRD systems can be applied at different wavelengths with simple designs. Another FLRD set-up was designed at visible region for chemical sensing with the gained experience. Schematic diagram of the set-up is demonstrated in Figure 18.

As a light source a four channel fiber coupled laser (12) was used. It provides four different wavelengths with temperature stability. Temperature and current of each wavelength channel can be controlled independently with control unit on the laser. It has  $< 5 \mu\text{s}$  rise/fall time and 80 kHz full modulation depth.

For the design of the FLRD set-up, 808 nm was selected as the working wavelength. The power of the light at this channel was around 20 mW. To obtain a sinusoidal modulation laser beam a function generator (15) that modulated the laser was used. Light was coupled into 2% leg of a 2x2 optical fiber coupler (13) with 98:2 split ratios. First, 190 meter fiber (14) was spliced to the 2% leg of the coupler and a second coupler was added to the set-up by splicing the other end of 190 meter fiber to the input fiber end of the coupler. Then, the 98% leg of the second coupler was spliced to the second input of the first coupler and fiber cavity was formed. Output signal was detected by a silicone PIN detector (16) from the 2% output of the second coupler and it was monitored by the digital oscilloscope. 98% leg of the first coupler was connected to the detector to provide a trigger level.

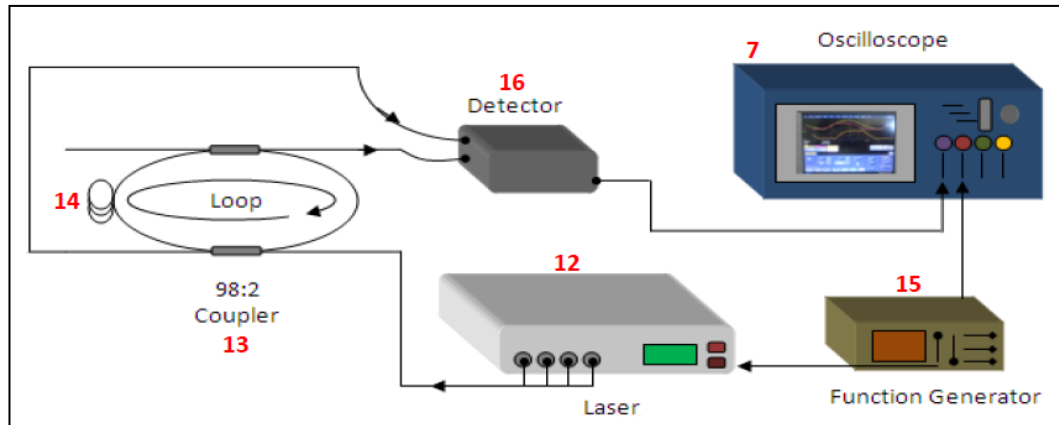


Figure 18. FLRD experimental set-up at visible region

98:2 split ratio was determined by modeling the light loss in the cavity from the given manufacturer loss parameters of fiber, couplers, etc. as shown in Table 3. For loop cycles between 20-34, 98:2 ratio works better than all the others.

Table 3. Optical loss calculations to modelize a coupler\*

| Coupler split ratio (%)  | Initial power<br>10000 $\mu$ W | Attenuation of fiber Nufern<br>780HP: 9 dB/km @642 nm |          |          |          | Fiber loss per round<br>(dB): 1,71 |          | Fiber length (190 m) |  |
|--------------------------|--------------------------------|---|----------|----------|----------|------------------------------------|----------|----------------------|--|
|                          | 1,00%                          | 2,00%   | 3,00%    | 4,00%    | 5,00%    | 10,00%                             | 20,00%   | 30%                  |  |
| Coupler split ratio (dB) | 0,043648                       | 0,087739  | 0,132283 | 0,177288 | 0,222764 | 0,457575                           | 0,9691   | 1,54902              |  |
| Rounds                   | 100                            | 200   | 300      | 400      | 500      | 1000                               | 2000     | 3000                 |  |
| 0                        |                                |   |          |          |          |                                    |          |                      |  |
| 5                        | 12,62851                       | 22,81869  | 30,89147 | 37,13405 | 41,80287 | 48,68835                           | 29,98678 | 11,83319             |  |
| 10                       | 1,594791                       | 2,603464  | 3,180943 | 3,447344 | 3,494959 | 2,370556                           | 0,449604 | 0,046675             |  |
| 15                       | 0,201398                       | 0,297038  | 0,327547 | 0,320035 | 0,292199 | 0,115418                           | 0,006741 | 0,000184             |  |
| 20                       | 0,025434                       | 0,03389   | 0,033728 | 0,02971  | 0,024429 | 0,00562                            | 0,000101 | 7,26E-07             |  |
| 25                       | 0,003212                       | 0,003867  | 0,003473 | 0,002758 | 0,002042 | 0,000274                           | 1,52E-06 | 2,86E-09             |  |
| 30                       | 0,000406                       | 0,000441  | 0,000358 | 0,000256 | 0,000171 | 1,33E-05                           | 2,27E-08 | 1,13E-11             |  |
| 35                       | 5,12E-05                       | 5,03E-05  | 3,68E-05 | 2,38E-05 | 1,43E-05 | 6,49E-07                           | 3,41E-10 | 4,46E-14             |  |
| 40                       | 6,47E-06                       | 5,74E-06  | 3,79E-06 | 2,21E-06 | 1,19E-06 | 3,16E-08                           | 5,11E-12 | 1,76E-16             |  |

\* Calculations were done by using Equation (2.3).



## CHAPTER 4

### RESULTS AND DISCUSSIONS

In this chapter, characterization of home-made FLRD systems will be discussed. Measurement results will be presented and a general discussion will be given for experimental improvements.

#### 4.1. FLRD SET-UPS at 1535 nm

In all the set-ups used in these studies a nanosecond pulsed laser source (1) with a center wavelength of 1535 nm was used. The laser light coupling to a fiber in all of the FLRD set-ups done by free space coupling technique using a pigtailed (one side fiber connected) collimator lens (2). The light coupling efficiency was monitored with a power meter placed at the fiber end of the lens. The laser power output is  $19.5 \pm 0.5 \text{ mW}$  and  $14.5 \pm 0.5 \text{ mW}$  of that (ca. 75%) was coupled to the fiber. The 99:1 coupler (3) was used as an input coupler to couple the laser light into the fiber cavity. The coupler split ratio is determined according to optical losses of fiber and insertion losses of the couplers. When a 99:1 coupler is used, only 1% of laser light is coupled into the cavity and the rest (99%) of the light was dumped. 1% leg of a second 99:1 coupler is used for monitoring the cavity loss during the ring down process. The rest of light (99%) is left in the cavity in this case. This results an (insertion) loss of  $20.47 \text{ dB}$  at the first coupler and  $0.17 \text{ dB} \times 2$  loss for each round trip in the cavity. Since the laser used is a  $4 \pm 1 \text{ ns}$  pulsed laser (light travels 20.8 cm in 1 ns in the fiber), which is much shorter than time required for a single round trip in the cavity, the choice of a cavity length is not important in this FLRD set-up so long as the cavity is not less than  $20.8 \times 5 \text{ cm}$ .

Once the FLRD set-up is complete, ring down signal was monitored and collected with a 1 GHz oscilloscope.

##### 4.1.1. Theoretical Results for the Closed FLRD Set-Up

In order to obtain a theoretic ring down time result, first  $A$  (total transmission loss) is calculated from fiber absorption and insertion losses of the couplers. The attenuation of the fiber is given as  $0.25 \text{ dB/km}$  by the manufacturer. Therefore, a 24 meter fiber used in the design of the cavity results in a loss of  $6.0 \times 10^{-3} \text{ dB}$ . The insertion loss of each coupler is  $0.17 \text{ dB}$  at 99% port, and for each round this value is duplicated since the set-up consists of two couplers. The total loss per round adds up to  $0.346 \text{ dB}$ ; sum of fiber absorption and insertion losses of two couplers. Then according to Equation (2.3) total transmission loss,  $A$ , is calculated as  $7.70\%$  as following;

$$-0.346 = 10 \log\left(\frac{P}{P_0}\right) \rightarrow \frac{P}{P_0} = 0.923$$

$$A(\text{percentage loss}) = 1 - 0.923 = 7.70 \times 10^{-2} = 7.70\%$$

Substitution of  $A$  into Equation (2.6) estimates the ring down time ( $\tau_0$ ) as  $1.50 \mu\text{s}$ . Here, the refractive index of the fiber is taken as 1.444 at 1535 nm.<sup>33</sup>

$$\tau_0 = \frac{nL}{cA} \rightarrow \tau_0 = \frac{1.444 \times 24 \text{ m}}{2.998 \times 10^8 \text{ ms}^{-1} \times 7.70/100} = 1.50 \mu\text{s}$$

And the round trip time,  $t_r$ , that is the time for a light to travel through the fiber loop cavity is calculated as  $115.5 \text{ ns}$ .

#### 4.1.2. Experimental Results for the Closed FLRD Set-Up

Ring down signals were recorded with InGaAs PIN detector and visualized on 1 GHz oscilloscope. The recorded output ring down signal and the peak amplitude vs time data are shown in Figure 19.

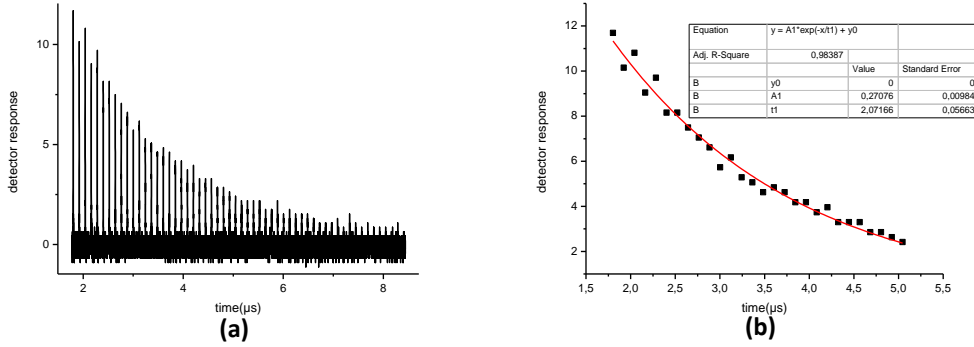


**Figure 19.** (a) Ring down signal and (b) fitted exponential decay obtained from the closed FLRD set up at 1535 nm

Pulse of the laser ( $4 \pm 1 \text{ ns}$ ) was much shorter than the round trip time,  $120 \pm 6 \text{ ns}$ . Therefore, the optical signal was detected as exponentially decaying pulses. In this way, successive trains can be obtained. The peak amplitude of each pulse is chosen to determine the laser light attenuation characteristics of the FLRD set-up. The peak amplitude values obtained from the ring down signal was fitted to a single exponential decay function that resulted the following fit equation;

$$I = 0.27076e^{-\left(\frac{t}{2.07166}\right)} \quad \text{Equation (4.1)}$$

In Equation (4.1)  $I$  is the light intensity in time ( $t$ ) domain. In this equation, ring down time,  $\tau_0$ , which is the time when the intensity is  $1/e$  of the initial value equals to  $2.07 \pm 0.06 \mu\text{s}$ . Time difference in any two pulse signals corresponds to the round trip time ( $t_r$ ) and measured as  $120 \pm 6 \text{ ns}$ . Optical fiber length can be determined from the round trip time. The length of the fiber is calculated as  $24.9 \pm 1.3 \text{ meters}$ . Then by using ring down time and the length of the fiber ( $L$ ), total transmission loss ( $A$ ) is calculated as  $5.79 \pm 0.33 \%$  where the refractive index of the fiber is taken as 1.4442 at 1535 nm. Finally, the total transmission loss in dB is calculated as  $0.26 \pm 0.03$ .

When theoretical and experimental results were compared, differences between fiber lengths, optical transmission losses, and ring down times can be seen. The difference in length of the fibers is due to the additional fiber parts such as fiber end of the collimating lens, fiber end of the connectors, etc. The theoretical optical loss ( $0.346 \text{ dB}$ ) was higher than the experimental loss ( $0.26 \pm 0.03$ ). This was expected because theoretical values were calculated with the manufacture reported maximum loss parameters of each component. For instance, the given fiber attenuation is  $0.25 \text{ dB/km}$ , whereas the actual losses were lower in our measurements. Therefore, it is normal to observe a slower decay and a higher ring down time compared to the theoretical values.

To optimize the FLRD set-up, measurements were repeated while several parameters like the position of the optical elements and the length of the fiber were changed. Some of these changes

resulted in extra optical losses and ring down time became lower. After all parameters were optimized as much as possible, effect of averaging of the pulse shots was determined by acquiring the data at different averages. The Table 4 presents the ring down times for averages from 1 to 100000 shots. The results show that an average of 100 is well enough to determine the ring down time within the accuracy of our system.

**Table 4.** Averaged pulse shots and resulted ring down times for closed FLRD set up

| Average shots number     | 1               | 10              | 100             | 1000            | 10000           | 100000          |
|--------------------------|-----------------|-----------------|-----------------|-----------------|-----------------|-----------------|
| Ring down time( $\mu$ s) | $1.55 \pm 0.06$ | $1.43 \pm 0.02$ | $1.33 \pm 0.03$ | $1.34 \pm 0.03$ | $1.33 \pm 0.03$ | $1.33 \pm 0.03$ |

Unfortunately, in the current set-up there were several problems like high peak intensity fluctuations and back reflections. To solve these problems the second coupler in the set-up was replaced with an optical isolator, which allows the light transmission in only one direction. Optical isolator used in the set-up has a single input, 99% output, and a 1% tap that is used to connect to the detector. After this alteration, ring down data was recorded, and peak amplitudes were fitted as the first case (Figure 20). The high amplitude fluctuations and (most of the) back reflections were cleaned. The significant improvements of R-square values from 0.98387 to 0.99933 and standard error from 0.05663 to  $6.28443 \times 10^{-3}$  was noted. As seen in the Figure 20, a much smoother ring down data was recorded.

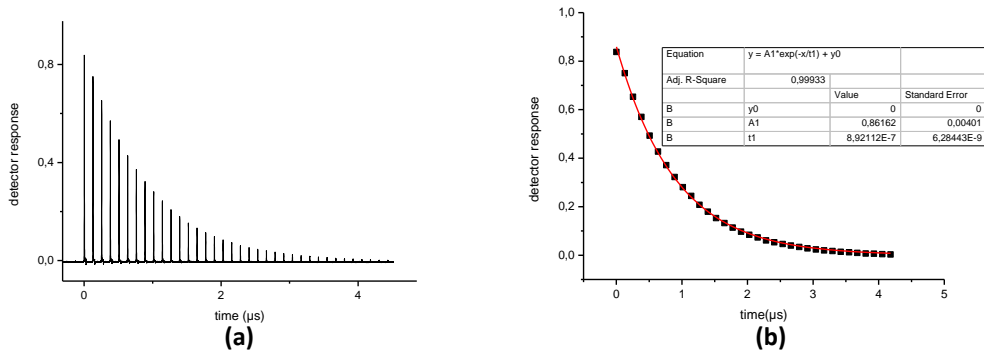


**Figure 20.** (a) Ring down signal and (b) fitted exponential light decay obtained from the closed FLRD set up at 1535 nm after the addition of isolator

With a similar treatment of the collected data, ring down time and round trip time of the new design were calculated as  $892 \pm 6$  ns and  $127 \pm 7$  ns, respectively. Decrease in ring down time is most probably because of increase in mechanical splice losses through the cavity during the replacement of coupler with the isolator. In addition, the insertion loss of the isolator is higher than the insertion loss of the coupler.

### 4.1.3. Experimental Results for the FLRD Set-up with Sensor Region Using Free Space Collimators

After the design of the sensor head with free space collimators ring down data was recorded before the introduction of a sample (Figure 21a). Distance between the collimators was set around 1.0 cm.

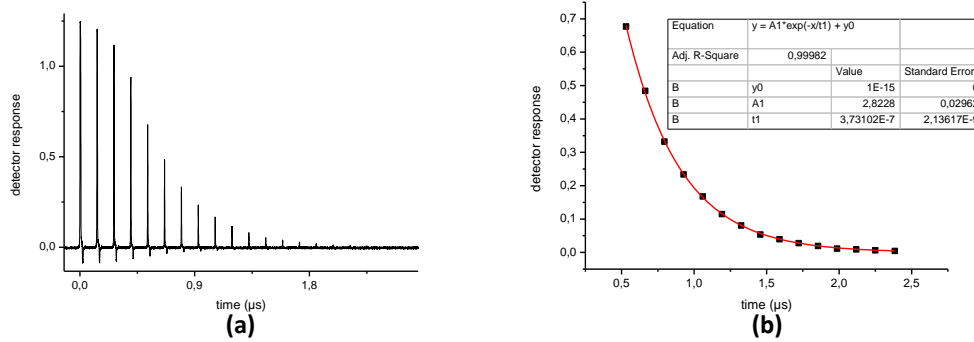
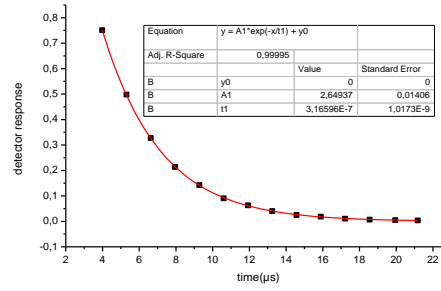
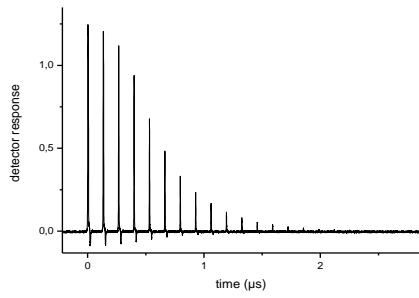


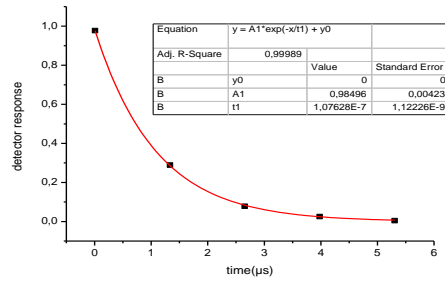
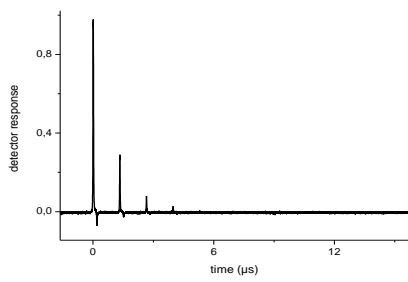
**Figure 21.** (a) Ring down signal and (b) fitted exponential light decay obtained from the FLRD set up at 1535 nm after addition of a sensor region using free space collimators

Ring down time was calculated as  $373 \pm 2 \text{ ns}$  from the fit equation of the exponential light decay in Figure 21b. We have noticed that the initial decay of the ring down corresponds to the nonlinear response of the detector due to saturation of the detector. Rapid decay of cladding mode may also have contributed to the observed response. Since the refractive index of the cladding is lower than the refractive index of the core, the light travels faster through the cladding. Therefore, this part of the data was not used during the fitting process.

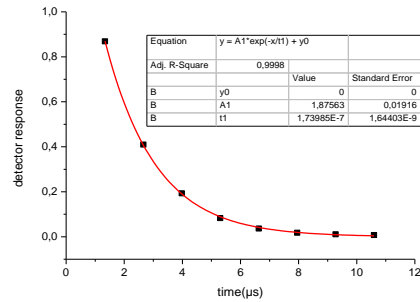
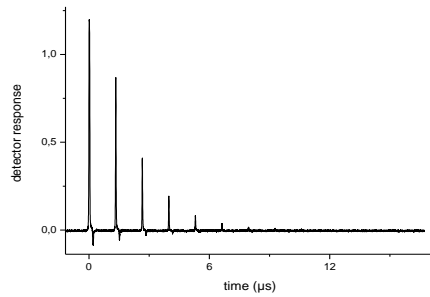
Sensor head design with collimators is suitable for solid sample measurements. With this aim, amorphous silicone thin films on glass surface provided by Physics Department-GUNAM Laboratory at Middle East Technical University were measured. These films were coated on glasses in nanometer thicknesses and used for production of solar cell. The collected data and their respective fitted ring down signals for a glass without film and for glasses coated with different thicknesses as 90 nm, 210 nm and, 390-410 nm are given in Figure 22.



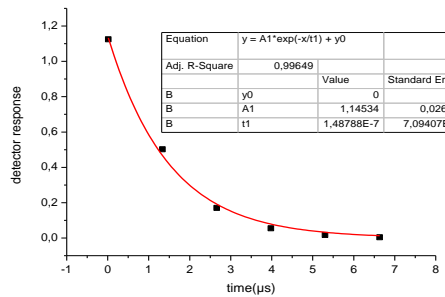
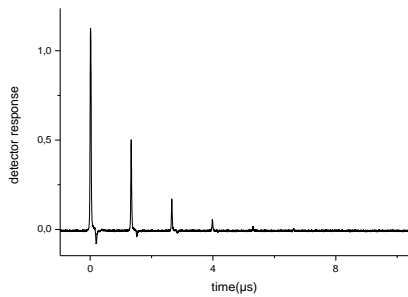
(a)



(b)



(c)



(d)

**Figure 22.** Fitted exponential light decays of FLRD set-up with sensor region after introduced sample a) 2.14 mm glass b) 90 nm silicone on 2.93 mm glass surface c) 210 nm silicone on 2.17 mm glass surface d) 390-410 nm silicone on 2.17 mm glass surface

The calculated ring down times of the samples are given in Table 5.

**Table 5.** Thicknesses of amorphous silicone thin films and resulted ring down times

| Thickness of amorphous silicone (nm) | Thickness of glass (mm) | Ring down time (ns)* | A                 |
|--------------------------------------|-------------------------|----------------------|-------------------|
| Reference                            | 2.14                    | $317 \pm 1$          | $0.41 \pm 0.03$   |
| 90                                   | 2.93                    | $108 \pm 1$          | —                 |
| 210                                  | 2.17                    | $174 \pm 2$          | $0.759 \pm 0.009$ |
| 390-410                              | 2.17                    | $149 \pm 7$          | $0.89 \pm 0.04$   |

\* Individual standard error of the measurement derived from the fitting

The significant decrease in the ring down time of the samples with silicone films relative to the reference glass shows that there was a significant absorption of amorphous silicone films. Since the thicknesses of the bare (uncoated) glass and the others were very different, the bare glass could not be used as a reference and a calibration curve cannot be obtained. Although a calibration curve for the successful thicknesses of amorphous silicone could not be achieved, results are distinct enough to say that an FLRD set-up can easily be configured for thickness measurement of thin films. Even though, the study provides experience for the measurements of thin films; enough amorphous silicone samples from Physics Department were not provided to complete the thickness measurement study with the FLRD technique.

#### 4.1.4. Experimental Results for the FLRD Set-Up with Sensor Region Using Ferrules

Sensor head configurations in FLRD systems can be altered according to phases of the samples. In the FLRD set-up free space collimators were replaced with ferrules for the measurements of strongly absorbing liquid samples in a narrower sample region. Ring down data was recorded with free space (air filled region) and ring down time was calculated as  $313 \pm 6$  ns from the fit equation of the exponential light decay in Figure 23. The saturated part of the signal was also not included during the data analysis, as before.

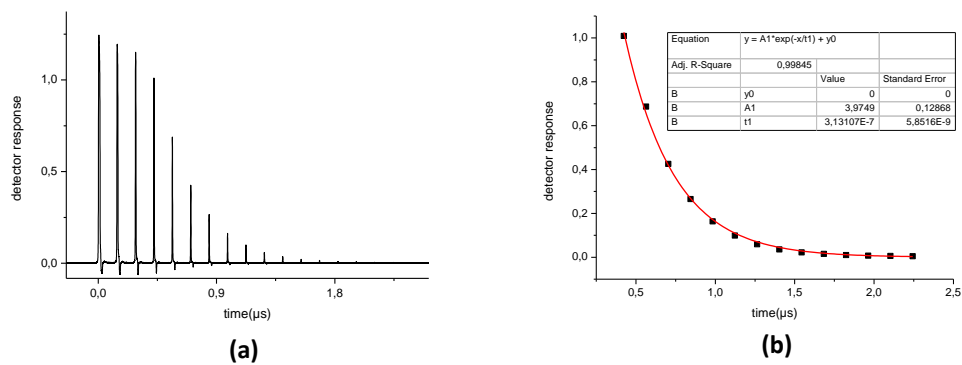


**Figure 23.** (a) Ring down signal and (b) fitted exponential light decay obtained from the FLRD set up at 1535 nm after addition of a sensor region using ferrules

After an iterative optimization by observing the light coupling between the ferrules, the distance between the ferrules was adjusted to 80  $\mu\text{m}$ . After the optimization of the set-up, various pure liquids were measured (Table 6). (Ring down data of the liquids are given in the Appendices.)

**Table 6. Ring down time results for different solvents introduced between two ferrules**

| <i>Sample</i>     | <i>Ring down time (ns)*</i> | <i>Absorption, A</i> | <i>Extinction coefficient, <math>\epsilon(\text{m}^{-1})</math></i> |
|-------------------|-----------------------------|----------------------|---|
| Air               | 313 $\pm$ 6                 | 0.447 $\pm$ 0.009    | -   |
| Isopropyl alcohol | 282 $\pm$ 3                 | 0.354 $\pm$ 0.003    | 1.44x10 <sup>3</sup> **   |
| n-butanol         | 274 $\pm$ 3                 | 0.497 $\pm$ 0.005    | (3.23 $\pm$ 0.08)x10 <sup>3</sup>                                   |
| n-hexane          | 293 $\pm$ 4                 | 0.511 $\pm$ 0.006    | (3.39 $\pm$ 0.09)x10 <sup>3</sup>                                   |
| Water             | 396 $\pm$ 3                 | 0.478 $\pm$ 0.007    | (3.0 $\pm$ 0.1)x10 <sup>3</sup>                                     |

\* Individual standard error of the measurement derived from the fitting

\*\*Jonasz M. (2006) 10.01.2013 <<http://www.tpdsci.com/tpc/AbsCfOfWaterDat.php>>

The ring down times of isopropyl alcohol, n-butanol and n-hexane are lower than the ring down time of air and water. On the other hand, ring down time of water is higher compared to air. The reason for this is the close refractive indexes of water and the ferrules. This results in less divergence when the beam exists the ferrules and increases the coupling of light to the second ferrule. In addition a non-polar solvents decahydronaphthaline (known as decalin, C<sub>10</sub>H<sub>18</sub>) was also investigated. Ring down times for decalin were recorded at different distances as 80, 60, 40  $\mu\text{m}$  between the ferrules with different averages of pulse shots.

Table 7 demonstrates the ring down time results for decalin when the distance was 80  $\mu\text{m}$  with 1, 16, 128, and 1024 pulse averages. However, repeated experimental results were not consistent with each other and ring down time decreases with time. When the measurements of air were repeated, there were differences in ring down times, too. The differences in ring down time of air show that we cannot reproduce the same environment after the sample measurement. In these experiments, in order to introduce the liquids in between the ferrules the distances between the ferrules were increased. These result suggest that we could not accurately adjust back the ferrules distance down to initial distance (80  $\mu\text{m}$ ), again. Instead of re-adjustment of the ferrule distances to introduce the sample, we decided to fix the distance and introduce the liquid from above and have the gravity to the trick of getting the liquid in between ferrules.

**Table 7.** Obtained ring down times for decalin (C<sub>10</sub>H<sub>18</sub>) introduced to the sample region (d=80 $\mu\text{m}$ )

| <i>Averaged pulse number</i> | <i>Ring down time (ns)*</i> |
|------------------------------|-----------------------------|
| 1                            | 208 $\pm$ 5                 |
| 16                           | 203 $\pm$ 1                 |
| 128                          | 162 $\pm$ 3                 |
| 1024                         | 166 $\pm$ 4                 |

\* Individual standard error of the measurement derived from the fitting

In this case instead of working with different liquids, we have decided to work with water since it had the highest ring down time in the previous measurement. We have prepared a saturated solution of fluorescein (C<sub>20</sub>H<sub>12</sub>O<sub>3</sub>) in water and diluted it 10 and 100 times. Fluorescein solutions were introduced to sample region of the FLRD set-up and ring down times were recorded (Table 8, Table 9, Table 10). In this experiment, distance between the ferrules was set to 80 μm and measurements were repeated three times. Water data was collected in between.

**Table 8.** First measurement results for fluorescein solutions (Set 1)

| <i>Sample</i>      | <i>Ring down time(ns)*</i> |
|--------------------|----------------------------|
| Air                | 163.7 ± 0.5                |
| Water              | 177.7 ± 0.5                |
| Diluted 100 times  | 178.6 ± 1.0                |
| Water              | 177.5 ± 1.0                |
| Diluted 10 times   | 178.0 ± 0.5                |
| Water              | 182.6 ± 1.1                |
| Saturated solution | 184.6 ± 1.2                |
| Water              | 185.2 ± 1.0                |

*\* Individual standard error of the measurement derived from the fitting*

**Table 9.** Second measurement results for fluorescein solutions (Set 2)

| <i>Sample</i>      | <i>Ring down time(ns)*</i> |
|--------------------|----------------------------|
| Air                | 161.2 ± 0.9                |
| Water              | 185.7 ± 1.3                |
| Diluted 100 times  | 169.9 ± 0.5                |
| Water              | 170.9 ± 0.6                |
| Diluted 10 times   | 174.8 ± 0.4                |
| Water              | 179.3 ± 0.8                |
| Saturated solution | 180.5 ± 0.9                |
| Air                | 157.1 ± 0.7                |
| Water              | 182.8 ± 0.8                |

*\* Individual standard error of the measurement derived from the fitting*

**Table 10.** Third measurement results for fluorescein solutions (Set 3)

| <i>Sample</i>      | <i>Ring down time(ns)*</i> |
|--------------------|----------------------------|
| Air                | 155.7 ± 0.4                |
| Water              | 169.6 ± 0.3                |
| Diluted 100 times  | 199.1 ± 0.5                |
| Air                | 155.3 ± 1.0                |
| Water              | 158.3 ± 0.8                |
| Diluted 10 times   | 176.1 ± 0.6                |
| Air                | 162.9 ± 0.5                |
| Water              | 149.7 ± 0.8                |
| Saturated solution | 179.1 ± 1.0                |
| Air                | 157.7 ± 0.6                |
| Water              | 149.4 ± 0.6                |

*\* Individual standard error of the measurement derived from the fitting*

In these fluorescein solution experiments the distance between the ferrules was not changed and liquid was introduced to the region by dropping to this narrow area. Air and water measurements between the initial and the last are also not consistent. Inability of the sensor region to measure a liquid prevented to reach precise results. These inabilities were originated from the physical design of the sensor region. We noticed that the area between the ferrules was not fully filled with the sample in some of the measurements. Another reason might be the insufficient cleaning and drying process between each measurement. In any one of these measurements, ring down times should not be greater than the pure water, which is the lower limit in concentration (none). In all sets, unexpected ring down times for fluorescein solutions were obtained. In some cases, the most diluted one resulted in highest absorption as  $169.9 \pm 0.5$ . The result may be derived from the previous problems as lack of cleaning and contact troubles. Unfortunately, due to the physical restrictions of our sensor region for fluid measurement, we could not reach reliable results. For reliable/reproducible results the sample region must be improved. To solve these problems we are working on a new flow cell design with fixed ferrules that would eliminate all the aforementioned problems and let to introduce the liquid samples continuously for easy cleaning.

#### **4.2. FLRD SET-UP at 808 nm**

Ultimate aim of the study is forming of absorption profiles for different trace chemicals at visible region. With the gained experience at 1535 nm set-up another FLRD set-up at visible region was constructed. As a light source 808 nm light of the laser was selected. Power of this channel was measured with the power meter as  $16 \pm 0.5 \text{ mW}$ , and the power from the 98% output of the first coupler was measured as  $15 \pm 0.5 \text{ mW}$ .

##### **4.2.1. Theoretical Loss Calculations for the Closed FLRD Set-up**

To calculate a theoretic ring down time value, total transmission loss ( $A$ ) per round was obtained from the sum of absorption of the fiber and insertion losses of the couplers. The reported attenuation of the fiber is  $3 \text{ dB/km}$  (much higher than the 1535 nm fiber) and the estimated attenuation for 192 meter fiber (190 meter fiber + 2 meter fiber coupler) is  $0.576 \text{ dB}$ . Insertion loss of each coupler at 98% leg is  $0.2 \text{ dB}$  for each round of the light within the cavity. The total transmission loss is calculated as  $0.976 \text{ dB}$  that is the sum of  $0.576 \text{ dB}$  and twice of  $0.2 \text{ dB}$ . This loss corresponds to a 20.13% intensity loss of light. Finally, ring down time ( $\tau_0$ ) is calculated as  $4.62 \mu\text{s}$  and round trip time ( $t_r$ ) is calculated as  $930.6 \text{ ns}$  with using length of the fiber ( $L$ ), and total transmission loss ( $A$ ), and with the refractive index as 1.4531.<sup>33</sup>

##### **4.2.2. Experimental Results for the Closed FLRD Set-up**

A novel FLRD set-up was designed at visible region with the aim of detection of trace chemicals. The laser is modulated to record the ring down trains on the laser pulses. The laser is modulated at  $80 \text{ kHz}$  ( $12.5 \mu\text{s}$ ) with a function generator. This value is the full depth modulation level of the laser. Thus higher modulation frequencies are impossible for the laser. Since the pulse width of the laser after modulation was  $12.5 \mu\text{s}$ , which is higher than the round trip time of the light within the cavity, ring down trains coincide the laser pulses as in Figure 24.

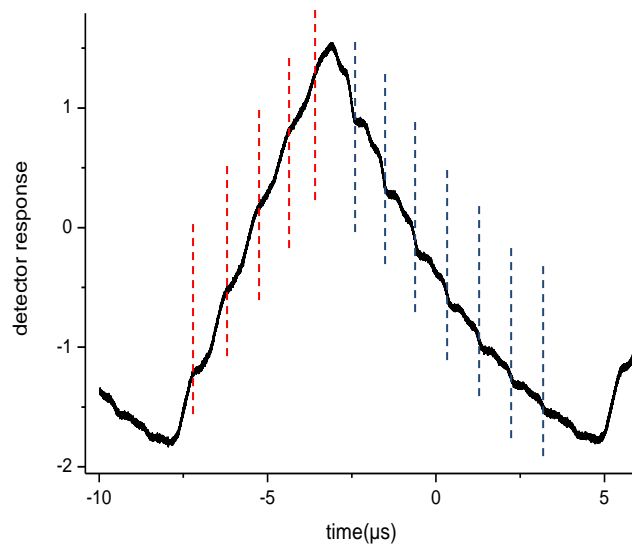


**Figure 24.** Recorded ring down trains riding on the laser pulse of the closed FLRD set up at 808 nm

Recorded signal in Figure 24 was consistent with steps. Observed steps for the initial parts (left side of the peak) were caused by time elapsed for a round trip before recombination of light with itself and the last part (right side of the peak) of the signal ring down trains were obtained. With the points where these steps observed could be used for the determination of the round trip time and the ring down times. Since the pulse train is on the laser pulse itself, it is very difficult to get the ring down times from these measurements. Instead, we decided to apply phase-shift method for the determination of ring down times.

To apply the phase shift method to the FLRD set-up, 98% leg of the first coupler (used as a reference, line in pink) and the 2% leg of the second coupler (light from the loop with leaking, line in yellow) were connected to a balanced Si PIN detectors. Phase shift derived from the cavity is easily seen in Figure 25 and 26.



**Figure 25.** Output signal of the reference laser light and light from the cavity

In order to characterize the FLRD set-up, data was recorded at several frequencies as 10, 30, 40, 50, 60 and 70 kHz. At 70 kHz, the phase shift is as in Figure 26. The rest are given in the Appendices. According to these results ring down time and the total absorption of the set-up can be calculated using Equation (1.7) defined in the Chapter 1.

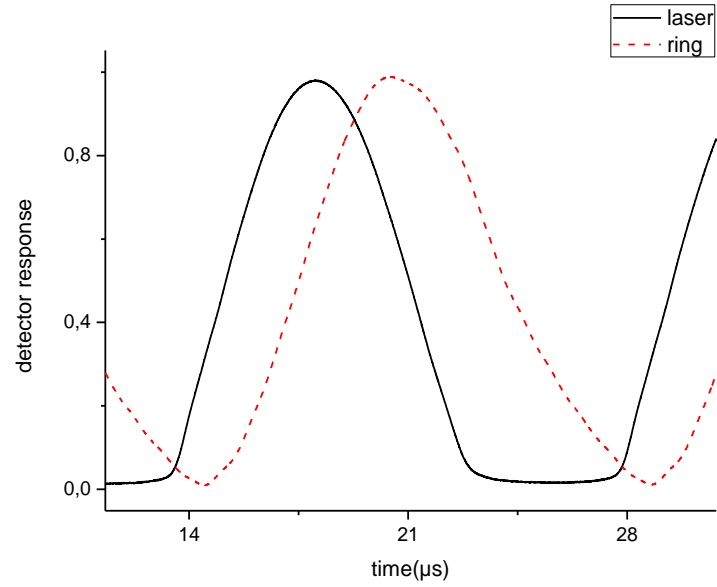


**Figure 26.** Output signal from the FLRD set-up after 70 kHz modulation of the laser (line in black demonstrates signal from the laser as a reference and line in red demonstrates the signal from the cavity)



## CHAPTER 5

### CONCLUSIONS

This thesis presents construction of two FLRD set-ups at 1535 nm and at 808 nm. At 1535 nm, a FLRD spectrometer set-up was designed with a pulsed laser source. A cavity was formed with optical fiber, a fiber coupler and an isolator, and an InGaAs PIN detector. Use of isolator in the cavity eliminated the observed intensity fluctuations and provided a smoother ring down signal. The obtained ring down time for the closed FLRD set-up was  $892 \pm 6$  ns. For solid sample measurements a sensor region was constructed using two free space collimators and ring down time was recorded as  $373 \pm 2$  ns. Thickness measurement of amorphous silicone thin films with different thicknesses on glass substrates was done. Even though a calibrated curve could not be obtained for sample films, the lower ring down times than the reference demonstrated that absorption occurs. When the thickness of the film becomes higher, absorption increases and rings down time decreases. We can say that our FLRD set-up can easily be configured for the measurements of thin film thickness at 1535 nm.

To detect liquid samples, another sensor region was designed with ferrules. When the optimization of the set-up was completed, a ring down signal was recorded ( $313 \pm 6$  ns) and total loss of the system was calculated relative to a reference. First, different pure liquids (water, isopropyl alcohol, n-hexane and n-butanol) were introduced to the region by dropping and ring down times were recorded. Fluorescein solutions in water with low concentrations were measured and data was recorded for the three measurement sets. During these measurements sensor region was not robust enough to obtain reliable measurements. Therefore, we could not obtain extinction coefficients from these measurements. A sensor region design with a flow cell design might be better for liquid measurements. In this way the contact and cleaning problems of the region will be eliminated.

With the gained experience at 1535 nm, another FLRD set-up was designed at visible-NIR region. The first step of the study was working on a single wavelength to characterize the set-up. The 808 nm light source of the multichannel laser along with two optical couplers and a section of fiber were used to design of the cavity. A Si PIN detector was used for the detection of the output signal. Unlike the set-up output at 1535 nm, the ring down signals were not in pulses since the pulse width is much larger than the fiber length in the cavity. Therefore, ring down trains were observed on the laser pulses. For this reason phase shift FLRD technique is more suitable and should be applied for the analysis of the output ring down signal. The phase shift calculations are much different than the pulsed ones and were not applied during this study.

To summarize, FLRD spectroscopy is a sensitive technique. The main advantages of the technique are easy configuration of the elements of the experimental set-up and adaptability for measurements of different phases of chemicals. We conclude that FLRD set-up at 1535 nm provided us great experience to get familiar with the technique and design a FLRD set-up. We applied our experience to a FLRD set-up at 808 nm as a first step for trace chemicals detection at visible-NIR region. With further developments, a low cost, simple, highly sensitive FLRD spectrometer can be utilized for various application areas at visible region.



## REFERENCES

1. McDonagh, C., Burke, C. S. & MacCraith, B. D. Optical Chemical Sensors. *Chemical Reviews* **108**, 400–422 (2008).
2. Barnes, J., Dreher, M., Plett, K., Brown, R.S., Crudden, C.M., Loock, H.-P. Chemical sensor based on a long-period fibre grating modified by a functionalized polydimethylsiloxane coating. *The Analyst* **133**, 1541 (2008).
3. Vallance, C. Innovations in cavity ringdown spectroscopy. *New Journal of Chemistry* **29**, 867–874 (2005).
4. O’Keefe, A. & Deacon, D. A. G. Cavity ring-down optical spectrometer for absorption measurements using pulsed laser sources. *Review of Scientific Instruments* **59**, 2544–2551 (1988).
5. Paldus, B. A., Harb, C.C., Spence, T.G., Wilke, B., Xie, J., Harris, J.S., Zare, R.N. Cavity-locked ring-down spectroscopy. *Journal of Applied Physics* **83**, 3991–3997 (1998).
6. Crouch, S., Skoog, D. A., West, D. M. & Holler, F. J. *Fundamentals of Analytical Chemistry*. (Brooks/Cole, USA 2003).
7. Wang, C. Fiber Loop Ringdown — a Time-Domain Sensing Technique for Multi-Function Fiber Optic Sensor Platforms: Current Status and Design Perspectives. *Sensors* **9**, 7595–7621 (2009).
8. Waechter, H., Litman, J., Cheung, A. H., Barnes, J. A. & Loock, H.-P. Chemical Sensing Using Fiber Cavity Ring-Down Spectroscopy. *Sensors* **10**, 1716–1742 (2010).
9. Tong, Z., Wright, A., McCormick, T., Li, R., Oleschuk, R.D. & Loock, H.-P. Phase-Shift Fiber-Loop Ring-Down Spectroscopy. *Analytical Chemistry* **76**, 6594–6599 (2004).
10. Kwok, M. A., Herbelin, J. M. & Ueunten, R. H. Cavity Phase Shift Method For High Reflectance Measurements At Mid-Infrared Wavelengths. *Optical Engineering* **21**, 216979–216979 (1982).
11. Herbelin, J. M. & McKay, J. A. Development of laser mirrors of very high reflectivity using the cavity-attenuated phase-shift method. *Applied Optics* **20**, 3341–3344 (1981).
12. Anderson, D. Z., Frisch, J. C. & Masser, C. S. Mirror reflectometer based on optical cavity decay time. *Applied Optics* **23**, 1238–1245 (1984).
13. Romanini, D. & Lehmann, K. K. Ring-down cavity absorption spectroscopy of the very weak HCN overtone bands with six, seven, and eight stretching quanta. *The Journal of Chemical Physics* **99**, 6287–6301 (1993).
14. Romanini, D. & Lehmann, K. K. Cavity ring-down overtone spectroscopy of HCN, H<sup>13</sup>CN and HC<sup>15</sup>N. *The Journal of Chemical Physics* **102**, 633–642 (1995).
15. Kotterer, M., Conceicao, J. & Maier, J. P. Cavity ringdown spectroscopy of molecular ions: A  $2\Pi_u \leftarrow X2\Sigma_g^+$  (6–0) transition of N<sub>2</sub><sup>+</sup>. *Chemical Physics Letters* **259**, 233–236 (1996).
16. Romanini, D., Kachanov, A. A., Sadeghi, N. & Stoeckel, F. CW cavity ring down spectroscopy. *Chemical Physics Letters* **264**, 316–322 (1997).
17. Duschinsky, F. The temporal progression of the intensity of intermittently excited resonance radiation. *Zeitschrift für Physik* **81**, 7–22 (1933).
18. Engeln, R., Von Helden, G., Berden, G. & Meijer, G. Phase shift cavity ring down absorption spectroscopy. *Chemical Physics Letters* **262**, 105–109 (1996).
19. Gupta, M., Jiao, H. & O’Keefe, A. Cavity-enhanced spectroscopy in optical fibers. *Optics Letters* **27**, 1878–1880 (2002).
20. Trefiak, N. R., Barnes, J., Rask, F., Courtney, D.G., Walford, R., Li, R., Oleschuk, R.D., Loock, H.-P. Absorption measurements in microfluidic devices using ring-down spectroscopy. *Proceedings SPIE, Photonic Applications in Biosensing and Imaging* **5969**, 00–00–9 (2005).
21. Stewart, G., Atherton, K., Yu, H. & Culshaw, B. An investigation of an optical fibre amplifier loop for intra-cavity and ring-down cavity loss measurements. *Measurement Science and Technology* **12**, 843–849 (2001).

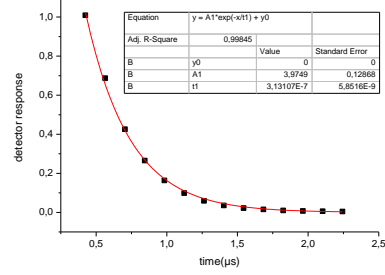
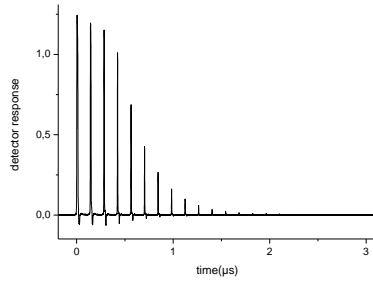
22. Brown, R. S., Kozin, I., Tong, Z., Oleschuk, R. D. & Loock, H.-P. Fiber-loop ring-down spectroscopy. *The Journal of Chemical Physics* **117**, 10444–10447 (2002).
23. Tong, Z., Jakubinek, M., Wright, A., Gillies, A. & Loock, H.-P. Fiber-loop ring-down spectroscopy: A sensitive absorption technique for small liquid samples. *Review of Scientific Instruments* **74**, 4818–4826 (2003).
24. Tarsa, P. B., Rabinowitz, P. & Lehmann, K. K. Evanescent field absorption in a passive optical fiber resonator using continuous-wave cavity ring-down spectroscopy. *Chemical Physics Letters* **383**, 297–303 (2004).
25. Wang, C. & Scherrer, S. T. Fiber Loop Ringdown for Physical Sensor Development: Pressure Sensor. *Applied Optics* **43**, 6458–6464 (2004).
26. Wang, C. Fiber ringdown temperature sensors. *Optical Engineering* **44**, 030503–030503 (2005).
27. Li, R., Loock, H.-P. & Oleschuk, R. D. Capillary Electrophoresis Absorption Detection Using Fiber-Loop Ring-Down Spectroscopy. *Analytical Chemistry* **78**, 5685–5692 (2006).
28. Waechter, H., Bescherer, K., Dürr, C. J., Oleschuk, R. D. & Loock, H.-P. 405 nm Absorption Detection in Nanoliter Volumes. *Analytical Chemistry* **81**, 9048–9054 (2009).
29. Rushworth, C. M., James, D., Lee, J. W. L. & Vallance, C. Top Notch Design for Fiber-Loop Cavity Ring-Down Spectroscopy. *Analytical Chemistry* **83**, 8492–8500 (2011).
30. Mitschke, F. *Fiber Optics: Physics and Technology*. (Springer, Berlin, 2009).
31. Pollock, C. *Fundamentals of Optoelectronics*. (McGraw-Hill Education, New York, 1994).
32. Ghatak, A. & Thyagarajan, K. *An Introduction to Fiber Optics*. (Cambridge University Press, USA, 1998).
33. Malitson, I. H. Interspecimen Comparison of the Refractive Index of Fused Silica. *Journal of the Optical Society of America* **55**, 1205 (1965).

## APPENDICES

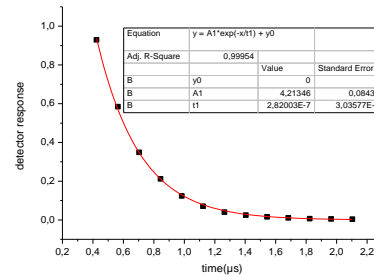
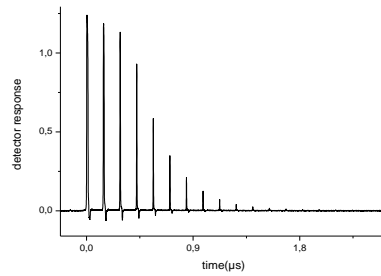
### A. Ring Down Signal Graphs

1. Ring down signals and fitted exponential light decay graphs for the results in Table 6.

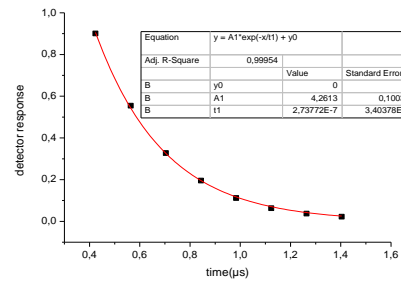
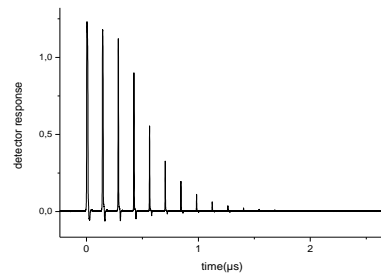
**Air:**



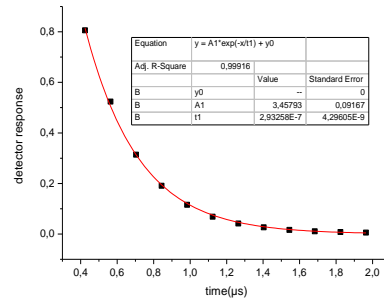
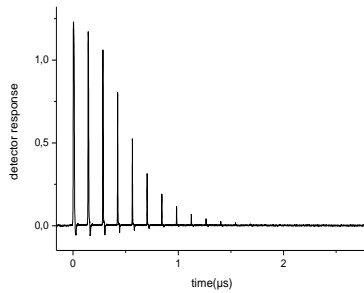
**Isopropyl alcohol:**



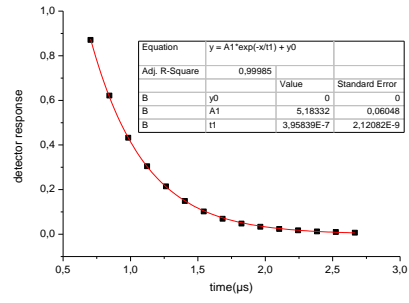
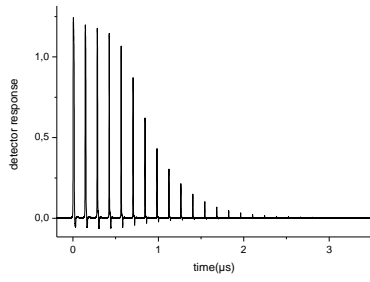
**n-butanol:**



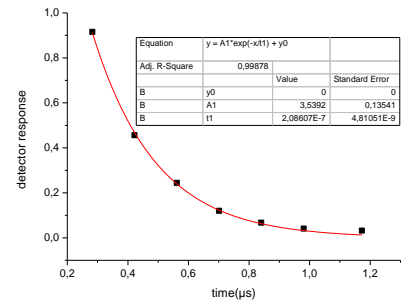
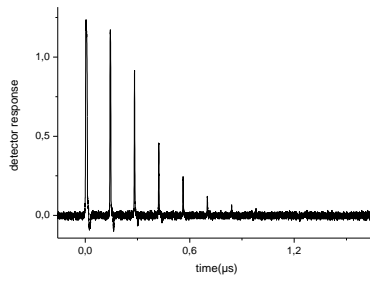
**n-hexane:**



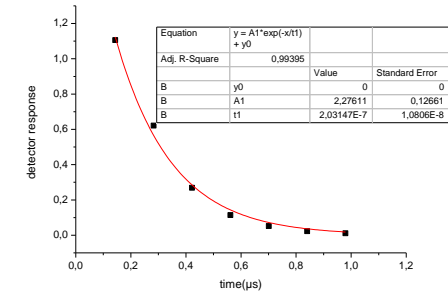
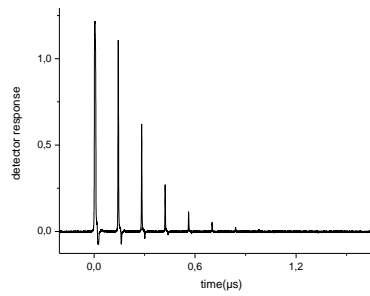
**Water:**



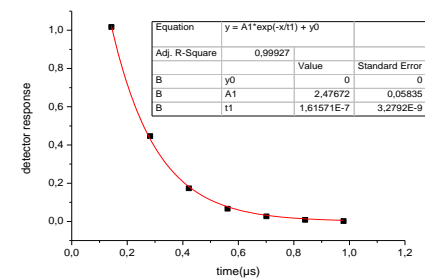
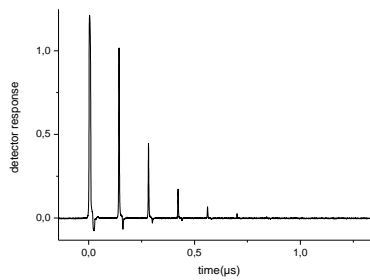
**2. Ring down signals and fitted exponential light decay graphs for the results in Table 7.  
1 average:**



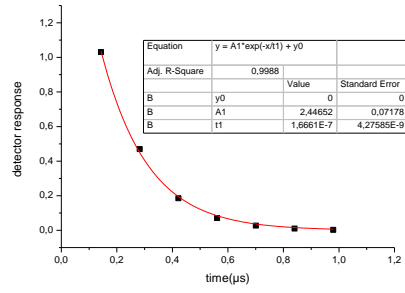
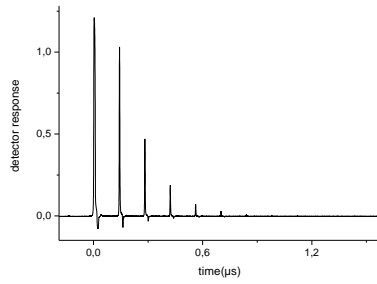
**16 average:**



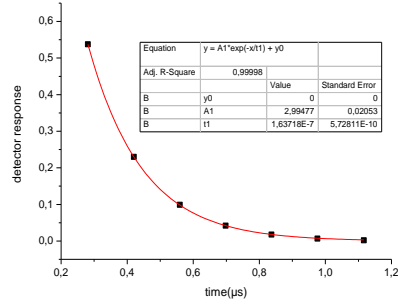
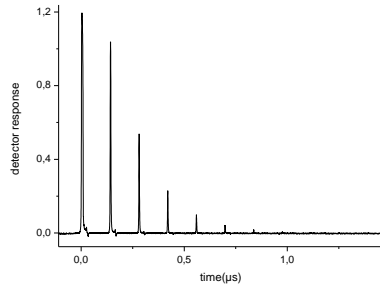
**128 average:**



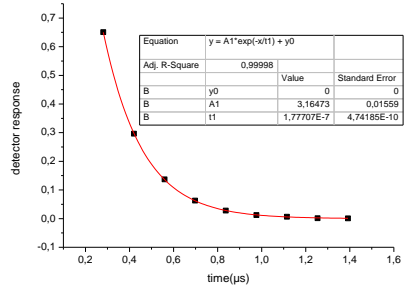
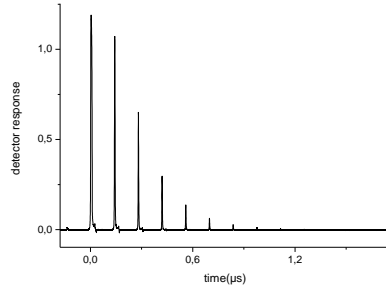
**1024 average:**



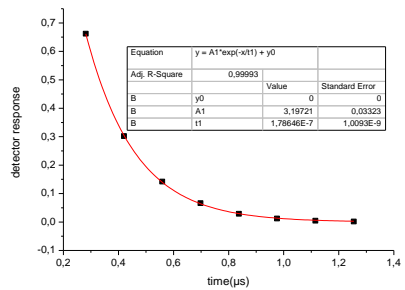
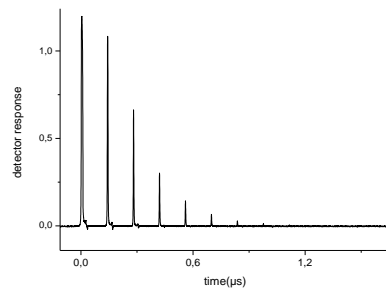
**3. First measurement result for fluorescein solutions (Set 1) (Table 8)  
Air:**



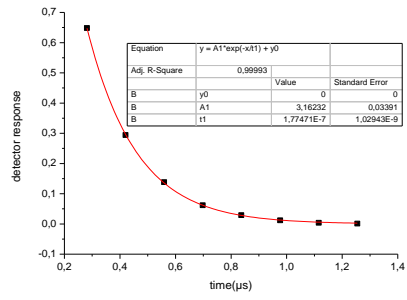
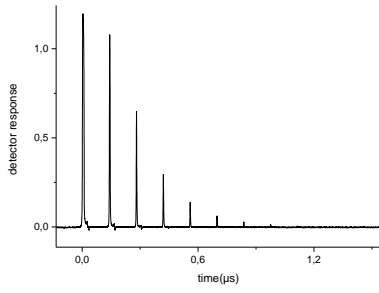
**Water:**



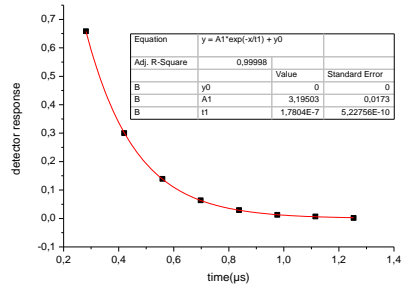
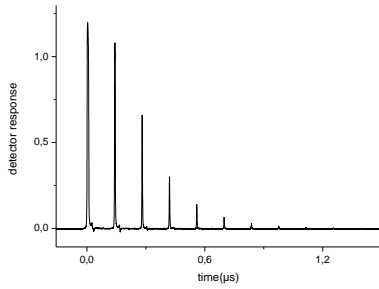
**Diluted 100 times:**



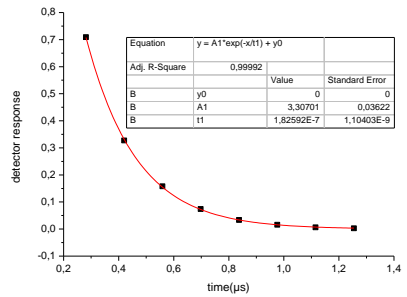
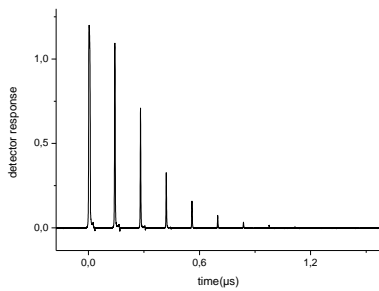
**Water:**



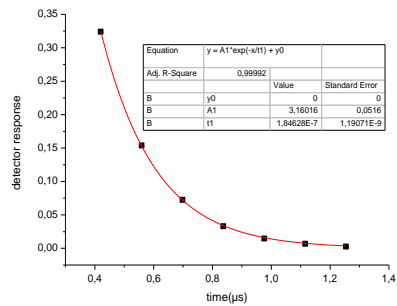
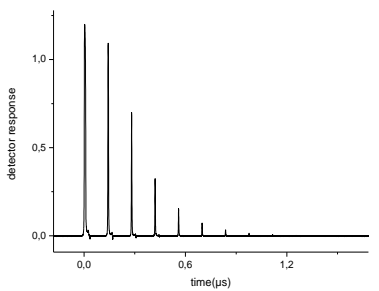
**Diluted 10 times:**



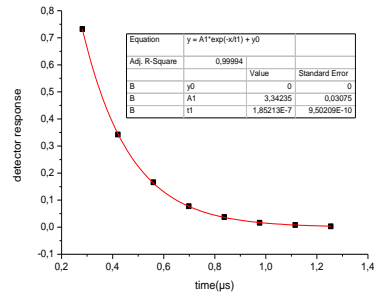
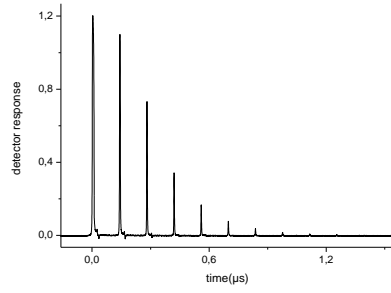
**Water:**



**Saturated solution:**

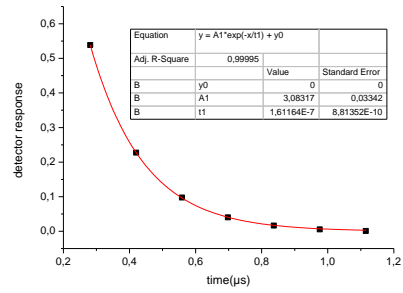
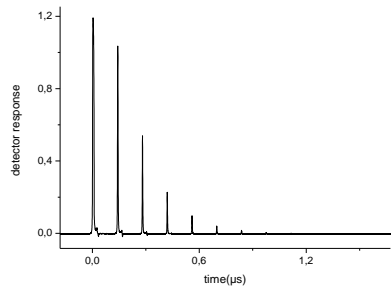


**Water:**

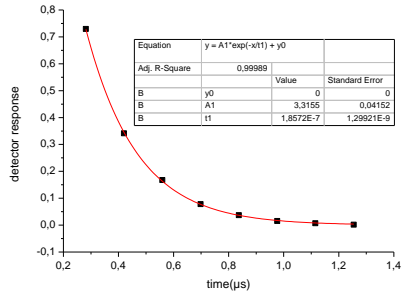
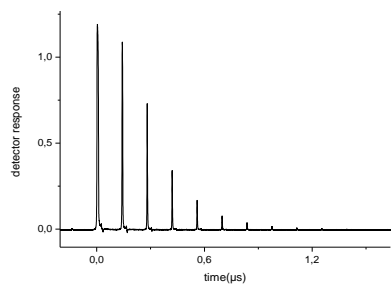


**4. Second measurement result for fluoresce in solutions (Set 2)(Table 9)**

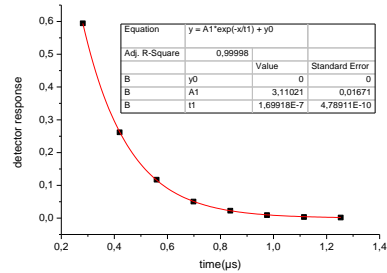
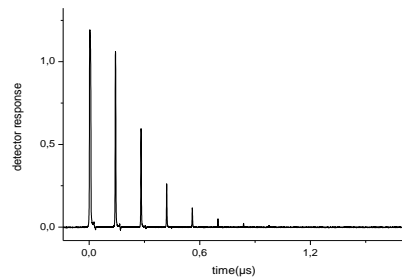
**Air:**



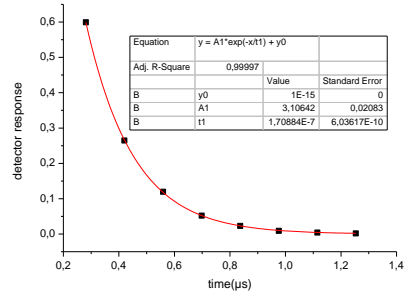
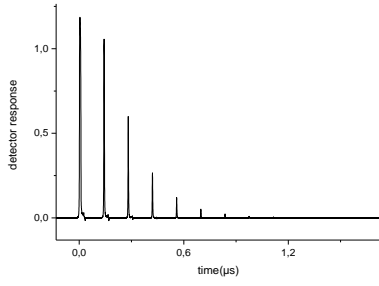
**Water:**



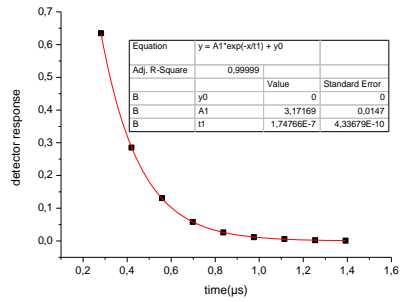
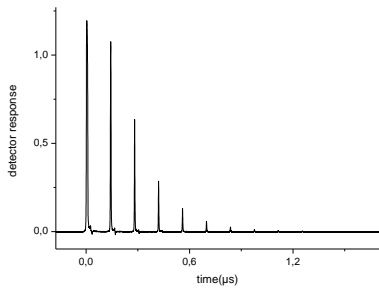
**Diluted 100 times:**



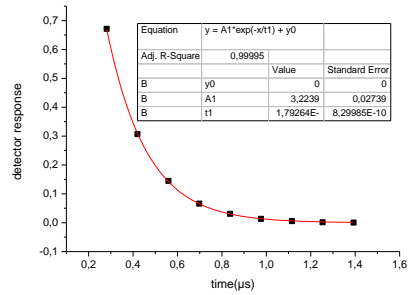
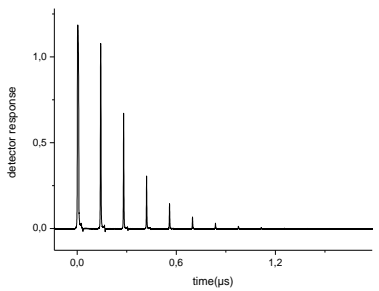
**Water:**



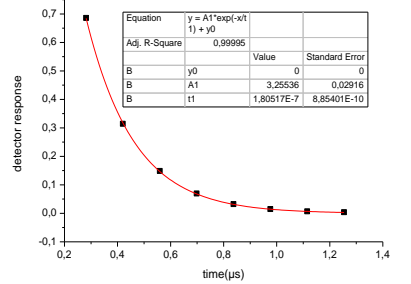
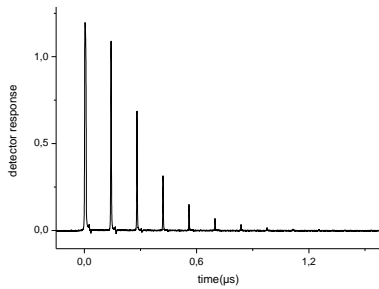
**Diluted 10 times:**



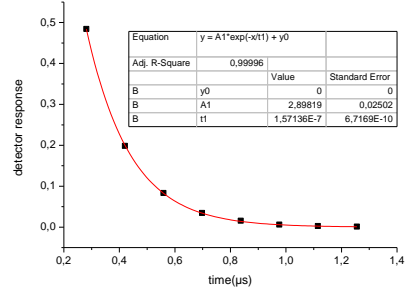
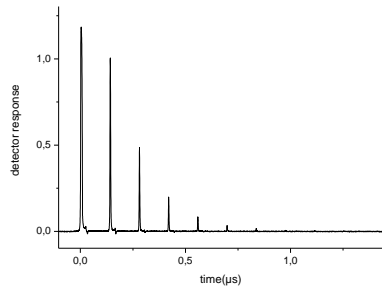
**Water:**



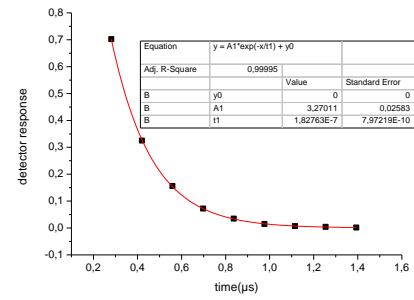
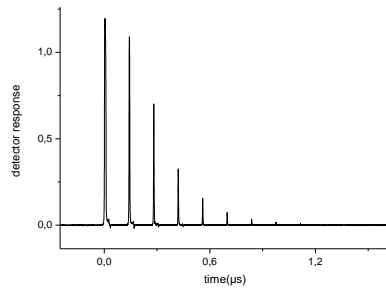
**Saturated solution:**



**Air:**

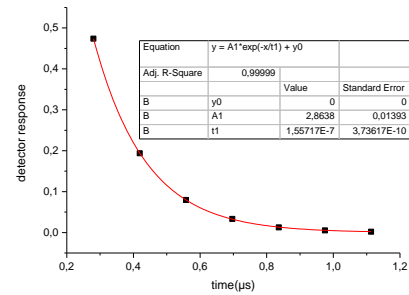
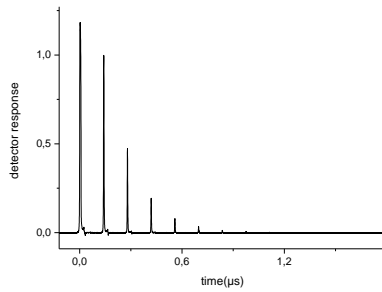


**Water:**

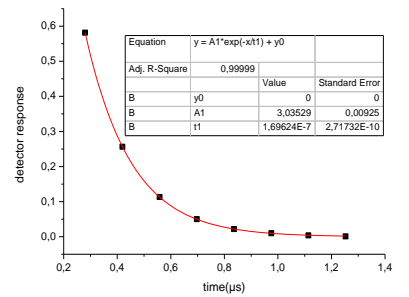
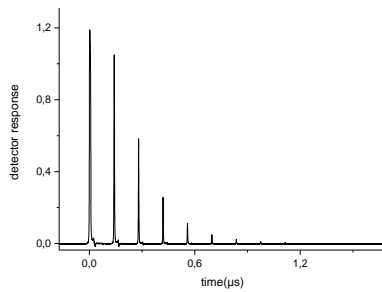


5. Third measurement result for fluorescein solutions (Set 3)(Table 10)

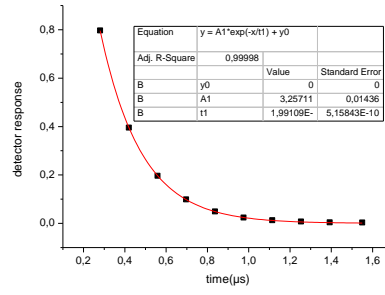
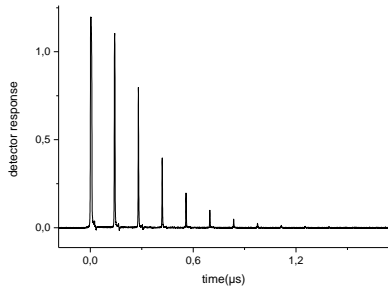
**Air:**



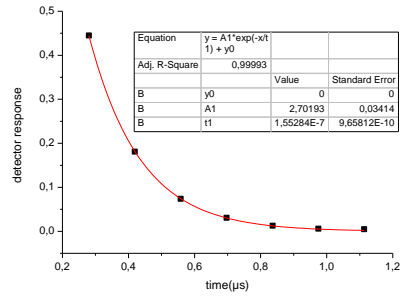
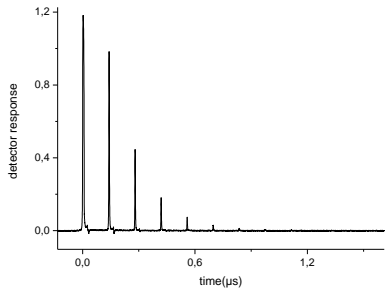
**Water:**



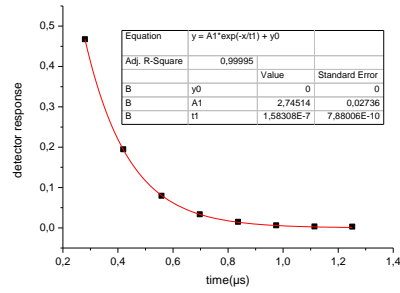
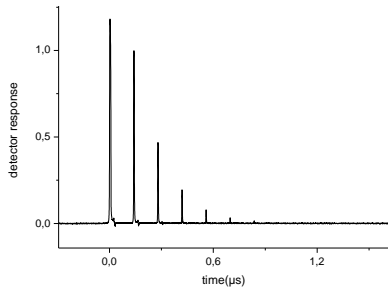
**Diluted 100 times:**



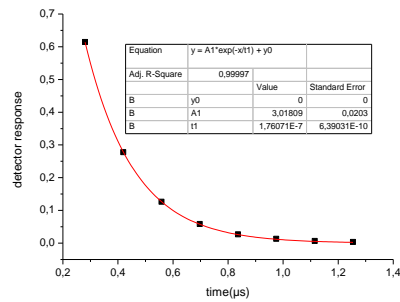
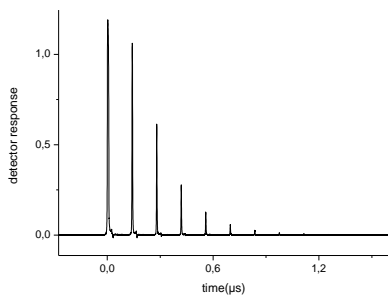
**Air:**



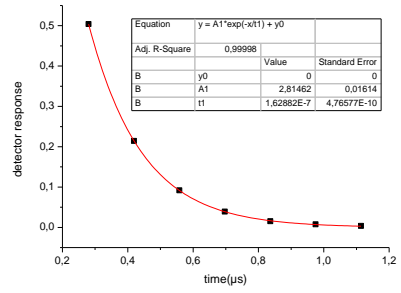
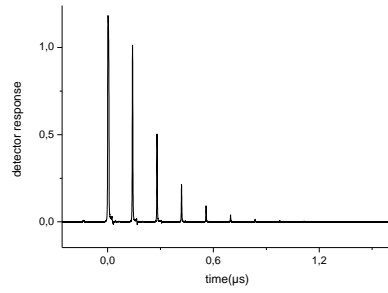
**Water:**



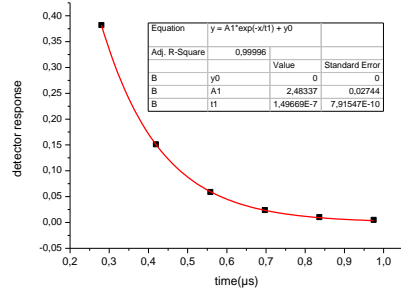
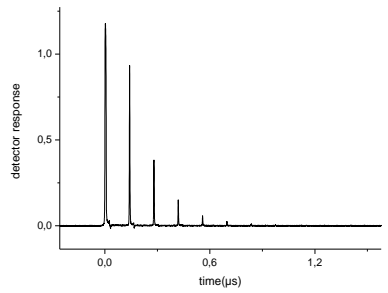
**Diluted 10 times:**



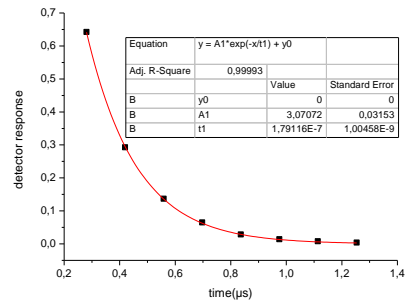
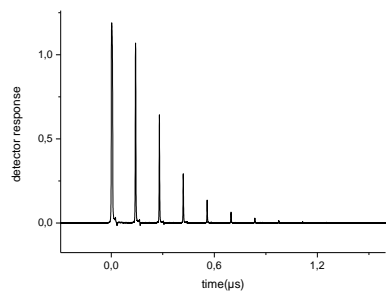
**Air:**



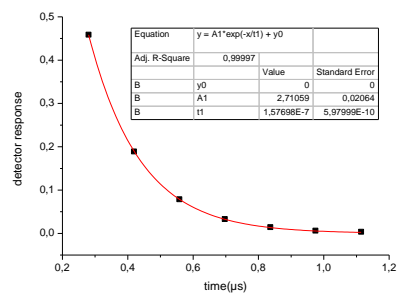
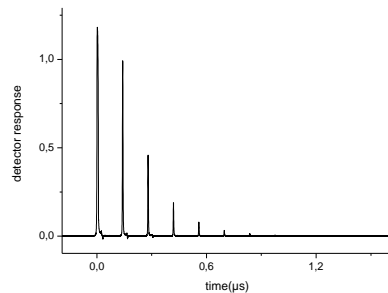
**Water:**



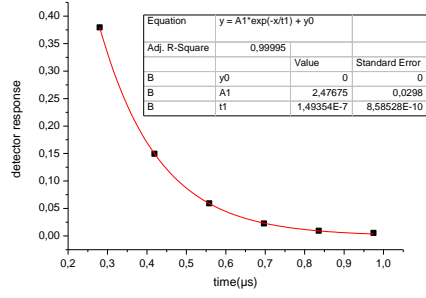
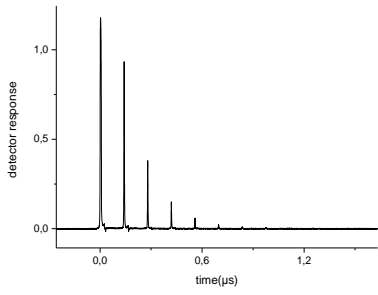
**Saturated solution:**



**Air:**

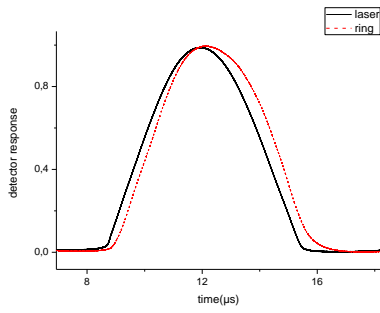


**Water:**

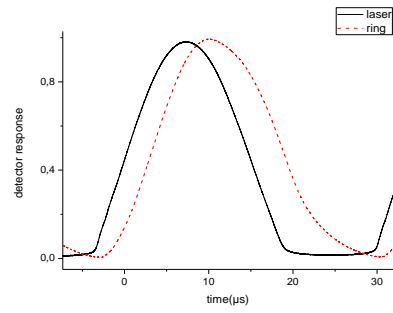


6. Output signals of the FLRD set-up at 808 nm with different frequencies.

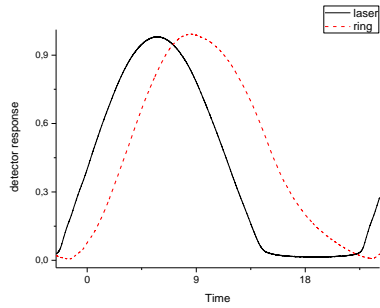
**10kHz:**



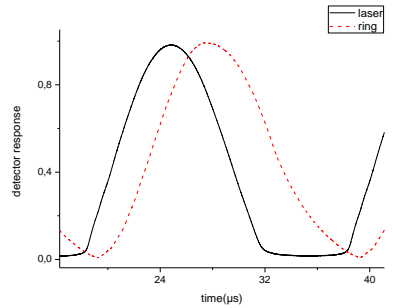
**30 kHz:**



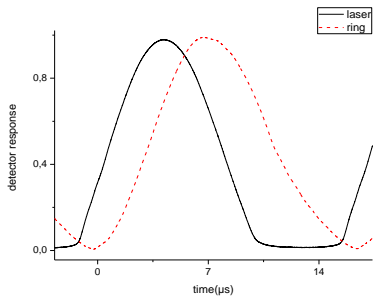
**40 kHz:**



**50 kHz:**



**60 kHz:**



**70 kHz:**

